

Morphodynamic zones and three-dimensional changes of the intertidal beach at Egmond aan Zee, the Netherlands



Marijn Celeste Boll
(3286096)

MSc Thesis Physical Geography
Track: Coastal Dynamics

Supervisor:
Prof. Dr. B.G. Ruessink

Department of Physical Geography
Faculty of Geosciences
Utrecht University
The Netherlands

March, 2014

Morphodynamic zones and three-dimensional changes of the intertidal beach at Egmond aan Zee, the Netherlands.

Marijn Celeste Boll (3286096)

MSc Thesis – March, 2014



Department of Physical Geography
Faculty of Geosciences
Utrecht University

Supervisor:
Prof. Dr. B.G. Ruessink

ABSTRACT

This thesis builds on the work of Price and Ruessink [T.D. Price, B.G. Ruessink., 2008. Morphodynamic zone variability on a microtidal barred beach. *Marine Geology* 251, 98-109] on the use of the relative occurrence of the morphodynamic zones to explain three-dimensional changes of the intertidal beach. A field campaign was conducted from 28 September to 31 October 2011 at Egmond aan Zee, the Netherlands, to map the intertidal beach morphology. It was found that low energetic wave conditions enhanced the intertidal morphology and caused onshore bar migration whereas high energetic wave conditions caused flattening of the intertidal morphology and offshore bar migration. Moreover, high energetic wave conditions with oblique incident waves were, in combination with an initial alongshore varying morphology, able to destruct the morphological pattern by the decay of a three-dimensional feature present in the initial beach morphology. The alongshore uniformity of the morphology and of the changes in morphology were tested using the approach of Plant et al. [N.G. Plant, R.A. Holman, and M.H. Freilich., 1999. A simple model for interannual sandbar behavior. *J. Geophys. Res.* 104, 15755-15776]. The alongshore uniformity of the morphology increased during low energetic wave conditions because morphological features, like the berm, bar and trough, enhanced. These morphological features did cause an increase in alongshore variation of the intertidal morphology, but their main pattern was shore parallel and induced, therefore, an increase in alongshore uniformity. The mapped morphology of the intertidal beach and a standard cross-shore wave transformation model coupled to an inner surf zone bore model were used to determine the morphodynamic zone distributions. The morphodynamic zone distributions showed an alongshore variation in intensity, induced by the alongshore variation of the initial morphology and caused, therefore, alongshore variation in the intertidal beach changes. It was found that, given the morphology, the alongshore variation in intensity of the morphodynamic zone distributions explain three-dimensional changes induced by the on/offshore bar migration and enhancing/flattening of the morphology. The destruction of the morphological pattern, induced by the decay of a three-dimensional feature, cannot be explained by the morphodynamic zone distribution as alongshore processes are involved.

CONTENTS

1	Introduction	6
2	Field site and data collection	10
2.1	Field site	10
2.2	Data collection and pre-processing	11
2.3	Boundary conditions	13
2.4	Selected periods and observations	14
3	Methodology.....	19
3.1	Alongshore uniformity	19
3.2	Morphodynamic zones.....	21
3.2.1	The cross-shore wave transformation model coupled to an inner surf zone model.....	21
3.2.2	The morphodynamic Boundaries.....	23
3.2.3	Model implementation	24
3.3	Accuracy analysis	25
4	Results.....	29
4.1	Spatial variability of the Digital Elevation and Difference Models.....	29
4.1.1	The perturbations of interest of the Digital Elevation Models	29
4.1.2	Alongshore uniformity	32
4.2	Morphodynamic zones.....	35
4.2.1	Distribution	35
4.2.2	Alongshore uniformity	39
4.2.3	The cross-shore relation between the morphodynamic zone distribution and Difference Model	39
4.2.4	Alongshore variability of the morphodynamic zone distributions	43
5	Conclusion.....	47
6	Recommendations	48
7	Bibliography	49

ACKNOWLEDGEMENT

First of all, I would like to thank Stefan Verschure and Joost Brinkkemper for making the fieldwork a very pleasant period and for all their help during the analysis and writing of this thesis. I would also want to express my gratitude to my parents for their unconditional love and support throughout my life. Special thanks go out to Niek Meijer for his love, support, and for putting up with my mood swings throughout this period.

1 INTRODUCTION

The intertidal beach is situated between mean low and mean high water level and is alternately submerged and exposed during every tidal cycle. It represents the pathway for sediment exchange between the near shore and the dry beach. Therefore, this part of the beach plays an important role in coastal protection. Seen against the background of future sea level rise due to climatic change, understanding the hydrodynamic and morphological processes at the intertidal beach is crucial.

The intertidal beach can be subdivided into three morphodynamic zones (Figure 1); the shoaling zone, the surf zone (with breakers and bores) and the swash zone (Masselink, 1993). These zones shift back and forth across the beach profile due to tidal water level variations and changes in the offshore wave condition. Consequently, any given point on the intertidal profile may be alternately dry, in the swash zone, the surf zone or in the shoaling wave zone if the tidal range is significant enough. Each zone is associated with characteristic hydrodynamic and sediment transport processes that depend on the wave condition (Masselink, 1993). The shoaling zone is the zone where incoming waves are affected by the seabed for the first time causing the waves to shoal (Figure 1). The wave speed and wavelength decrease and the wave height increases due to compensation of the energy per unit area of the wave. Shoaling waves are characterized by a larger onshore than offshore wave orbital velocity, i.e. the waves are skewed. The skewed waves generally have an onshore sediment transport with increasing transport rates towards the wave breakpoint.

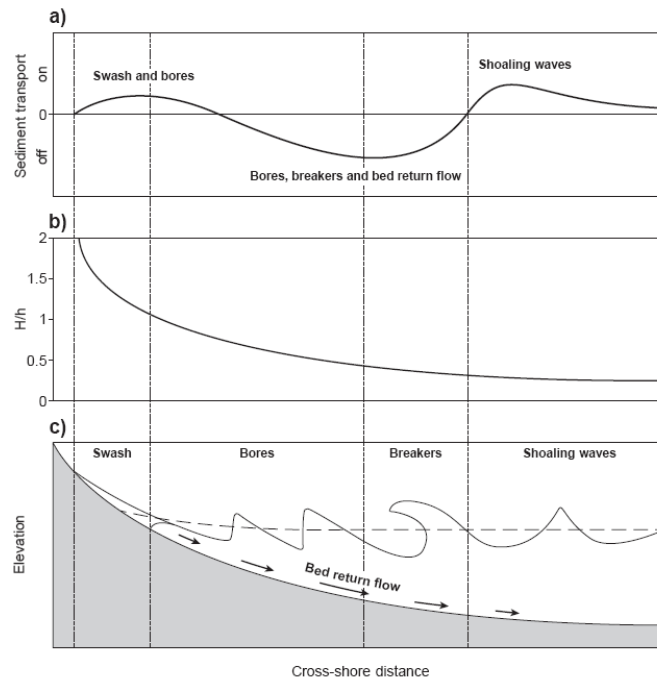


Figure 1. Cross-shore definition sketch of wave-induced processes and cross-shore sediment transport over a flat sloping beach. The sediment transport rate and direction (a), the relative wave height H_m/h (b) and the sloping beach and dominant wave-related processes (c). The dashed line in figure 1c represent the wave set-up profile. (Masselink et al., 2006).

Further onshore, waves break. The cross-shore sediment transport under breakers is caused by the relative contributions of onshore-directed transport by wave skewness and asymmetry. The offshore-directed transport by the bed return flow is called *undertow*. During severe breaking conditions the net sediment transport is offshore, as a result of the prevailing undertow. During weakly breaking conditions the net sediment transport can be onshore due to wave skewness. After the breaking point, the waves transform in turbulent bores, characterized by

a saw-tooth shape (Figure 1). The undertow still ensures offshore sediment transport, but the transport can be onshore during low-energy conditions. Swash is present where surf zone bores collapse on the beach (Figure 1). The swash zone can be defined as the region of the foreshore that is intermittently either wet or dry as a result of the action of the run-up and run-down (Butt et al., 2004). Swash causes sedimentation during relatively calm conditions due to a weak bias in uprush-driven transport. Under storm conditions, the backwash is often a much more efficient transporter of sediment than the uprush, resulting in net erosion.

The morphodynamic zones are based upon cross-shore processes. The relative occurrence of these zones controls both the evolution of the beach profile (Masselink, 1993) and the migration of intertidal bars (Price & Ruessink, 2008). Price and Ruessink (2008) calculated the relative occurrence and distribution of the morphodynamic zones for a cross-shore profile at the beach of Egmond aan Zee, the Netherlands. Between 13 October and 15 October 2005, the offshore wave height remained below 1m and the intertidal bar migrated onshore (Figure 2b). The onshore migration was caused by swash and surf processes (Figure 2a). Surf processes are mainly characterized by offshore sediment transport due to the undertow. However, visible inspections by Price and Ruessink (2008) showed that most surf zone conditions corresponded to surf zone bores propagating across the bar, as the water level decreased. The onshore orbital motion under the bores is considerably stronger than the offshore wave stroke (Aagaard et al., 2006), resulting in onshore sediment transport. The beach face steepened and the onshore directed sediment transport at $x < 20\text{m}$ was primarily caused by swash processes, while the offshore sediment transport between $x = 25\text{m}$ and $x = 45\text{m}$ was induced predominantly by breaking waves (Figure 2a).

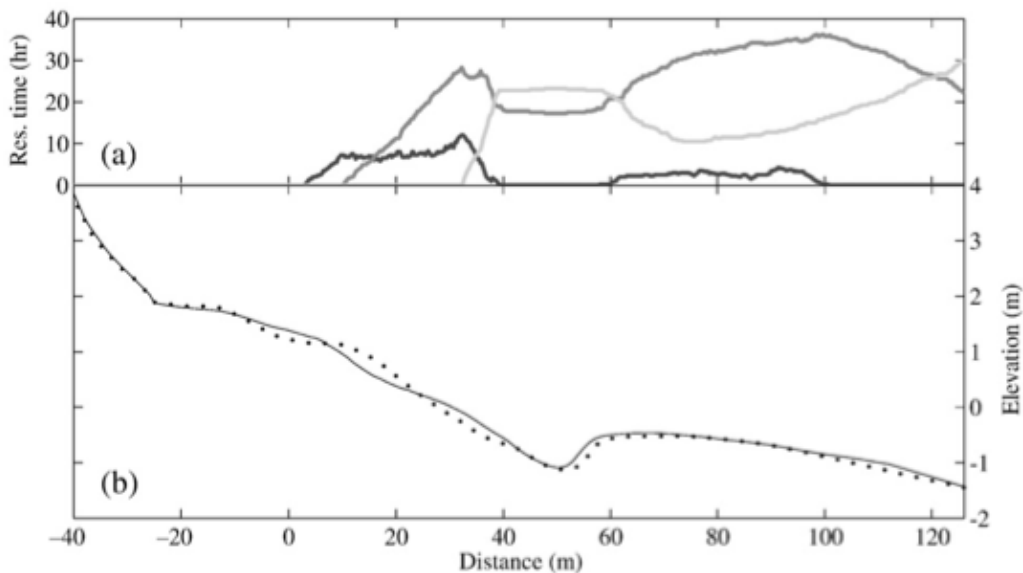


Figure 2. Predicted residence times (a) of the swash zone (dark gray), surf zone (medium gray) and shoaling zone (light gray) for 13 to 15 October 2005 and (b) beach profile elevation on 13 October (dotted line) and 15 October 2005. The maximum offshore wave height was 1.1m. (Price & Ruessink, 2008).

After the relatively calm period, a storm arrived between 25 and 26 October with wave heights exceeding 2m. The beach face flattened and the intertidal bar migrated offshore and became rather subdued (Figure 3b). The upper beach face eroded predominantly during swash conditions, while the intertidal bar migrated offshore by wave breaking and the associated undertow. The water levels during the storm were significantly higher than during calm conditions, preventing the occurrence of swash processes on the seaward side of the intertidal bar (Figure 3a).

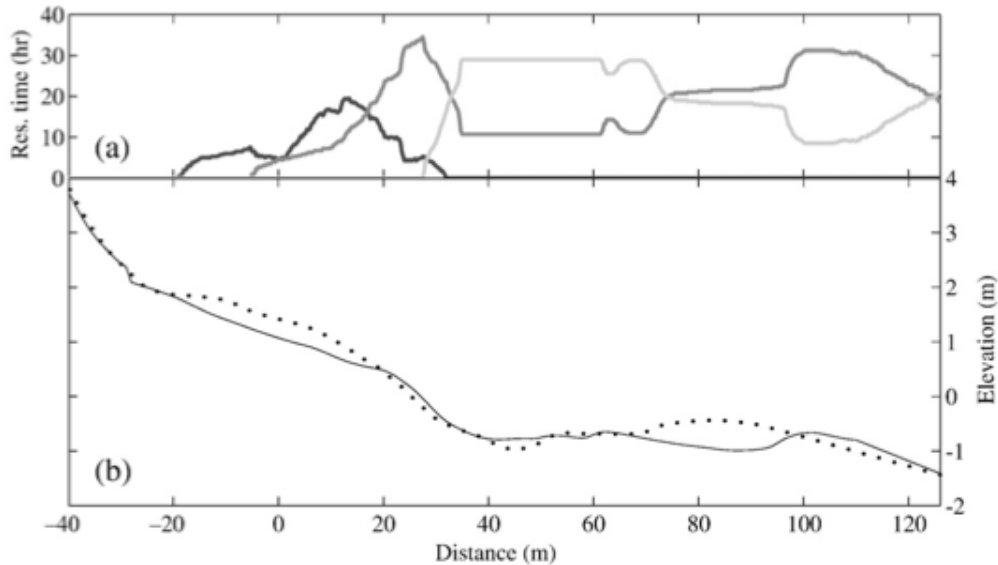


Figure 3. a) Predicted residence times of the swash zone (dark gray), surf zone (medium gray) and shoaling zone (light gray) for 25 to 26 October 2005 and b) beach profile elevation on 25 October (dotted line) and 26 October 2005. The maximum offshore wave height was 2.4m. (Price & Ruessink, 2008).

The relative occurrence of morphodynamic zones explains two-dimensional changes, as these behave alongshore uniform; like the on- and offshore bar migration. Furthermore, Price and Ruessink (2008) assumed an alongshore uniform (i.e. two-dimensional) beach morphology, as one cross-shore profile represents the entire intertidal beach. However, the intertidal beach may also show alongshore variations in morphology (i.e. three-dimensional morphology) aside from alongshore non-uniform changes in morphology (i.e. three-dimensional changes) (Ruessink et al., 2000). These alongshore variations are collectively referred to as *rhythmic features*. Rhythmic features are (quasi-) regular alongshore variations (i.e. three-dimensional features) with varying length scales. Most commonly along barred sandy coasts are rip channels. These appear as cross-shore depressions in shore-parallel sand bars. Other rhythmic features cause variations in the waterline like cusplets, cusps and shoreline sand waves. Three-dimensional changes in morphology can be caused by the alongshore redistribution of sand during the development of these three-dimensional features and the related alongshore movement (Short, 1985; Ruessink et al., 2000; Ruessink & Van Enckevort, 2003). The forcing mechanism behind the development and movement of these three-dimensional features are strong alongshore currents generated by oblique incident waves (Sonu & Russell, 1967). Three-dimensional changes in intertidal beach morphology may also occur due to alongshore variation in intensity of cross-shore processes, assuming an initial three-dimensional morphology.

If the relative occurrence of morphodynamic zones explains two-dimensional changes for a single cross-shore profile (Price & Ruessink, 2008), then three-dimensional changes may be explained by consecutive profiles and the distribution of morphodynamic zones. The aim of this study is therefore to determine if three-dimensional changes of the intertidal beach can be explained by the morphodynamic zone distribution. The following hypotheses are put forward:

- Three-dimensional changes induced by three-dimensional features cannot be explained by the morphodynamic zone distribution because alongshore processes are involved, and the morphodynamic zone approach only comprises cross-shore processes.
- The morphodynamic zone distribution can explain three dimensional changes induced by alongshore variation in intensity of cross-shore processes.

The hypotheses are tested by answering the questions below in the following sections. The main question for this research is:

1. Can three-dimensional changes in intertidal beach morphology be explained by the distribution of the relative occurrence of morphodynamic zones?

The following sub-questions are derived to answer the main question:

2. What are the changes in intertidal beach morphology?
3. Are these changes two-dimensional or three-dimensional?
4. Can the morphological changes be explained by the morphodynamic zone distribution?

Fieldwork was conducted at Egmond aan Zee, located along the Dutch coast, to map changes in intertidal beach morphology over a 6-week period. The beach morphology was mapped by a RTK-GPS to make digital elevation models (DEM's) and the changes in morphology between surveys were displayed in Difference Models (DM's). In order to determine whether the morphological changes of the intertidal beach were three-dimensional or two-dimensional the alongshore uniformity was tested, using the methodology of Plant et al. (1999). The corresponding morphodynamic zone distribution was then determined with a standard cross-shore wave transformation model coupled to an inner surf zone model, and then compared to the observed changes.

This report describes all aspects of the research, starting with a description of the field site and the data collection after which the selected periods for the research are presented (section 2). The methodology in section 3 describes the approach of Plant et al. (1999) in more detail, followed by the description and analysis of the standard cross-shore wave transformation model coupled to an inner surf zone model. To maintain readability and avoid many cross-references, it was chosen to combine the presentation of the results with the discussion in section 4. Finally, conclusions are drawn in section 5.

2 FIELD SITE AND DATA COLLECTION

A field experiment was conducted from 28 September to 31 October 2011 at the intertidal beach of Egmond aan Zee, the Netherlands. The field site is described in section 2.1 after which the data collection and pre-processing are explained in section 2.2. Section 2.3 describes the offshore wave conditions during the field campaign and finally, the observations of the three periods that were selected for further analysis are presented in section 2.4.

2.1 FIELD SITE

A field experiment was conducted from 28 September to 31 October 2011 at the intertidal beach of Egmond aan Zee, the Netherlands. The coast of Egmond aan Zee is north-south orientated and experiences a semi-diurnal tide, with a 1.4m and 2.1m tidal range during neap and spring tides respectively. The tidal curve is asymmetric with a 4-hour flood period and an 8-hour ebb-period. It is a barred system with two intertidal bars. The shoreline is exposed to waves with a southwestern to northern direction. The offshore wave height is 1.2m on average, with a mean period of 4.0s to 5.0s (Aagaard et al., 2005). The wave height can reach up to 5.0m during storms, especially when the waves are incident from the north-west (Price & Ruessink, 2008). The specific research area stretches over a 500m long shore by 100m cross-shore part of the intertidal beach, from the foot of the dunes to the low water line. At the southern border of the research area, a 48m high tower is located with an Argus video system. This system captures images of the intertidal beach of Egmond aan Zee every 30 minutes (Figure 4).



Figure 4. Image from Argus Tower on 14 October 2011, 13:30 hr with the cross-shore and alongshore driven pattern.

2.2 DATA COLLECTION AND PRE-PROCESSING

In order to determine the morphological changes of the intertidal beach, the bathymetry of the field site was mapped every other day during low tide with an RTK-GPS mounted on a quad motorcycle. Elevations were measured with a frequency of 10Hz and an average quad speed of 10 km/hr. The quad drove alongshore and cross-shore transects spaced 5m in order to get the alongshore as well as the cross-shore morphological features (Figure 4). The elevation data was converted to a local coordinate system, with beach post 41.250, near the Argus tower, as origin. The x-axis was orientated positive in seaward direction and the y-axis in southern direction. A manual cross-shore elevation profile of the fore dune was made in the middle of the study area ($y = -275\text{m}$, Figure 5). This dune profile, between $x = -20\text{m}$ and $x = -60\text{m}$, was assumed to be alongshore uniform for the entire fieldwork area.

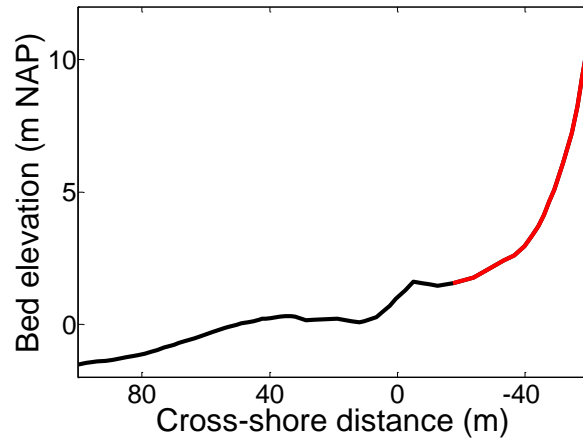


Figure 5. Cross-shore profile at $y = -275\text{m}$ on 29 September 2011. The dune elevation between $x = -20\text{m}$ to $x = -60\text{m}$ (red line) was assumed to be alongshore uniform for the entire research area.

The elevation data was interpolated on a regular grid using the Quadratic Loess method, which is a scale controlled interpolation method (Plant et al., 2002). With this method, weighted least squares were used to fit quadratic functions of the predictors at the center of neighborhoods to smoothen the data (Cleveland & Devlin, 1988). The radius of each neighborhood was chosen in cross-shore (λ_x) as well as in alongshore (λ_y) direction. The λ_x and λ_y are also referred to as smoothening parameters, as they determine the amount of detail in the data set. If λ is too large the bathymetry will fade out morphological features of interest, but if λ is too small the interpolated data will have a lot of fluctuations (i.e. noise), making it difficult to detect the main morphology. In this research the λ_x was set to 7.5m and λ_y to 40m.

The interpolated elevation data ranged from $x = 80\text{m}$ to $x = 20\text{m}$ with a grid size of 2.5m, the y-axis ranged from $y = -500\text{m}$ to $y = -50\text{m}$ with a grid size of 10m. The interpolated data $Z(x, y)$ formed a digital elevation model (DEM) for each survey (Figure 9c,d, Figure 10c,d and Figure 11c,d). By subtracting two consecutive surveys a difference model (DM) was created, displaying the changes in morphology for a certain period (Figure 9e, Figure 10e and Figure 11e):

$$Z(x, y)_{t2} - Z(x, y)_{t1} = \Delta Z(x, y)_{\Delta t}. \quad (1)$$

A few Difference Models showed a bias in elevation, as there was an unnatural elevation shift visible between the northern and the southern part of the field site, with the transition at exactly the center of the area (an example is shown in Figure 6). This offset error was created by differences in weight between the two quad operators, resulting in a difference in RTK-GPS base height. In order to correct these surveys the average elevation was calculated for the northern and southern side of the research area and together with previous and subsequent

DEM comparison, profile comparison and field observations the northern or southern part of the data was corrected by subtracting the difference in average elevation between the northern and the southern part of the fieldwork area. Table 1 shows the corrections that were made.

Table 1. The day, date, area and correction for the Difference Models.

Day	Date	Area	Δz_{mean} (m)
16	14-10-2011	North	-0.27
18	16-10-2011	South	-0.12
19	17-10-2011	North	-0.30
23	21-10-2011	North	-0.10
27	25-10-2011	South	-0.08

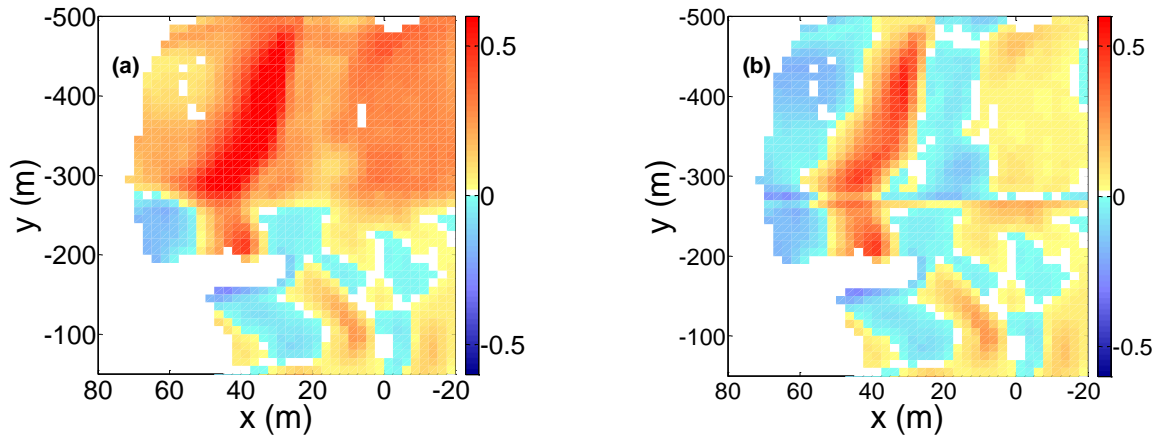


Figure 6. The Difference Model between fieldwork day 14 and 16 (12 October 2011 and 14 October 2011) with (a) offset error and (b) the corrected Difference Model.

2.3 BOUNDARY CONDITIONS

Offshore wave height and wave period were obtained by the Stroommeetpaal IJmond, located 2 to 2.5 km offshore from IJmuiden. The offshore angle of incidence was measured by a different buoy: the Munitiestort IJmuiden 1, located 16-16.5 km offshore. The field campaign started with a relatively long period of low energetic wave conditions after which two periods with high energetic wave conditions arrived with significant wave heights up to almost 4m (Figure 7). The offshore located buoy measured offshore directed waves during the period with low energetic waves and are therefore not representative for the wave conditions at the intertidal beach. Throughout the field campaign tidal water level variations were around 2m and obtained as hourly values computed by averaging the recordings of the tidal stations Petten Zuid and IJmuiden, which are separated alongshore by 30km and centered around Egmond aan Zee. All offshore variables were interpolated over time with an interval of 15 minutes and missing data was repaired by linear interpolation.

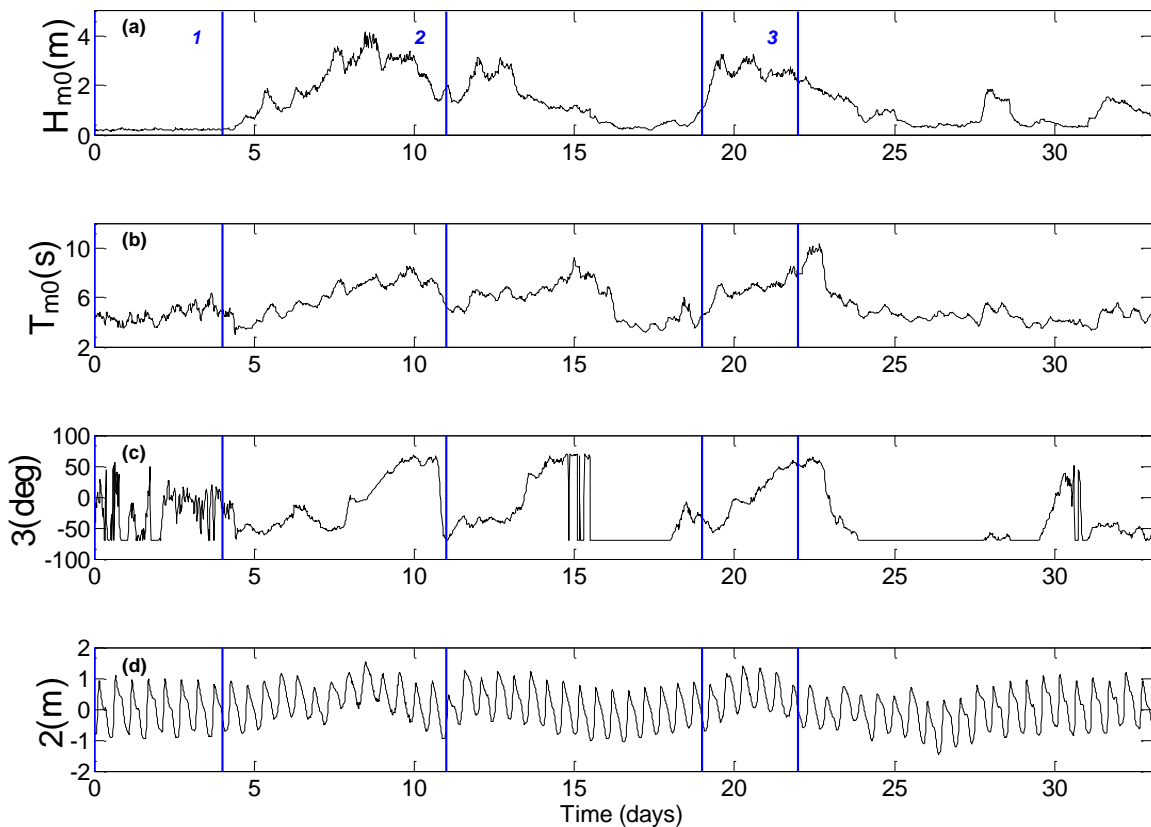


Figure 7. Offshore wave conditions and water levels during the field campaign. From top to bottom, the wave height (a), wave period (b), offshore angle of incidence with respect to shore normal (c) and measured water levels (e). The time axis is in days with the first day of the field campaign as $t=0$.

2.4 SELECTED PERIODS AND OBSERVATIONS

Three periods were selected from the collected data set for further analysis (Figure 7 and Table 2). The selection procedure was based on data availability and wave height. In this section, the changes of the intertidal beach morphology during these three selected periods are discussed in order to answer the first sub-question of this research: *What are the changes in intertidal beach morphology?* (section 1).

Table 2. The day of the beginning and the end of the three periods and the corresponding relative wave height, H_{m0} (m), and period, T_{m0} (s).

Period	Begin (day)	End (day)	H_{m0} (m)	H_{m0} mean (m)	T_{m0} mean (s)
1.	0	4	<0.45	0.2	4.6
2.	4	11	<4.0	1.9	6.0
3.	19	22	<3.5	2.5	6.6

The first period started at the beginning of the fieldwork and ended at day 4, just before the first storm of the year arrived. The period was characterized by low-energetic wave conditions (Figure 7). As mentioned earlier, the beach initially showed a typical summer morphology with a relatively steep beach face, with a slope $\tan(\beta) = 0.1096$, and a wide beach with a large berm that remained throughout this period. An intertidal bar was present with an accreted new bar on top that remained throughout the period. Figure 9a and Figure 9b show the new (lighter) intertidal bar on top of the old intertidal bar, whose color was darker as it contained more water due to its relatively lower elevation. A runnel was present landward of the intertidal bar with two major rip channels in the northern and southern part of the field site. The overall morphology of the fieldwork area remained more or less unchanged during the first period, and only a few small morphological changes were observed (Figure 9e). There were a clear alongshore erosion and sedimentation patterns visible at the beach face (between $x = 0\text{m}$ and $x = -20\text{m}$) as sediment was transported from the lower to the upper beach face, slightly increasing the beach face slope to $\tan(\beta) = 0.1120$. The same process was also visible at the new intertidal bar, where eroded sediment of the seaward side was deposited on top and over the intertidal bar (between $x = 0\text{m}$ and $x = 20\text{m}$). This caused the intertidal bar to migrate onshore. The erosion on the landward side of the intertidal bar is only visible in the northern part of the fieldwork area as the southern bathymetry measurements did not extend seaward enough (Figure 8 and Figure 9).

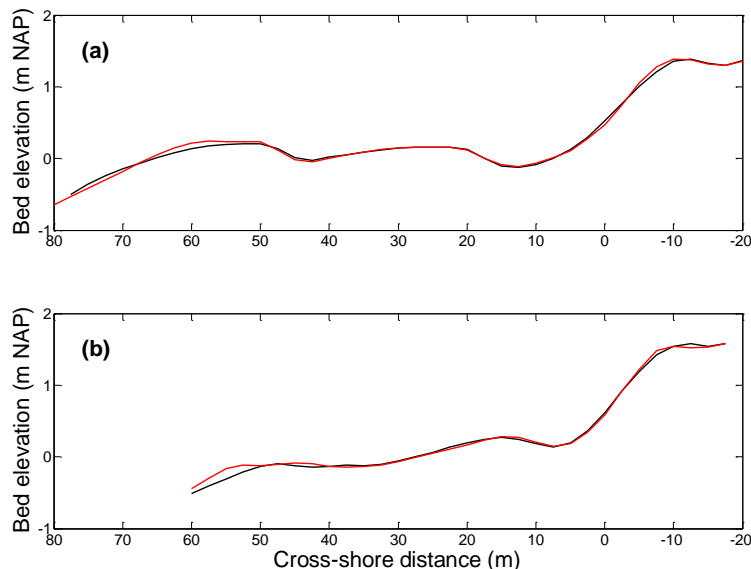


Figure 8. The cross shore profile at (a) $y = -400\text{m}$ and (b) $y = -200\text{m}$ at the beginning (black line) and end (red line) of the first period.

Period 2 comprised the transition of a relatively long period of low energetic wave conditions to the first high energetic wave condition of the season. The wave height increased up to almost 4m with an average wave height of 1.90m (Table 2). The first day of the second period equaled the last day of the first period (day 4) and the period ended after the peak of the storm on day 11. The storm caused an overall smoothing of the morphology. The summer berm eroded and the sediment was deposited in the runnel and on the lower beach face (Figure 10). As a result, the beach face became wider and the beach face slope decreased from $\tan(\beta) = 0.1120$ to $\tan(\beta) = 0.0367$. The intertidal bar flattened and migrated offshore, as did the position of the runnel. There were still two rip channels visible after the storm on more or less the same position as before the storm but less developed and the orientation of southern rip channel changed from east-west to a more north-south direction.

The last period, Period 3, consisted of a 4-day storm between day 19 and 22 (Figure 7). The wave height increased relatively fast from 0.5m to almost 3.5m and remained quite high throughout this period, with an average wave height of 2.5m (Table 2). The relatively calm conditions between Period 2 and 3 had caused the intertidal bar to migrate onshore and the beach face to steepen slightly from $\tan(\beta) = 0.0367$ to $\tan(\beta) = 0.0377$. In some places a even small berm arose. Furthermore, a intertidal bar was present at the beginning of Period 3, intersected by two rip channels and bounded landward by a runnel. Although the morphology had evolved between Period 2 and 3, it was not as developed as at the beginning of Period 1 and 2. The initial morphology of Period 3 had a 'winter profile' with a relatively wide beach, and a flat beach face and subdued intertidal bar. The second storm caused, just like during Period 2, an overall smoothing of the morphology (Figure 11). The slope of the beach face decreased to $\tan(\beta) = 0.0325$ and the intertidal bar flattened and migrated offshore, as did the runnel. Sedimentation took place in the runnel and in the rip channels, which eventually led to the disappearance of the southern rip channel.

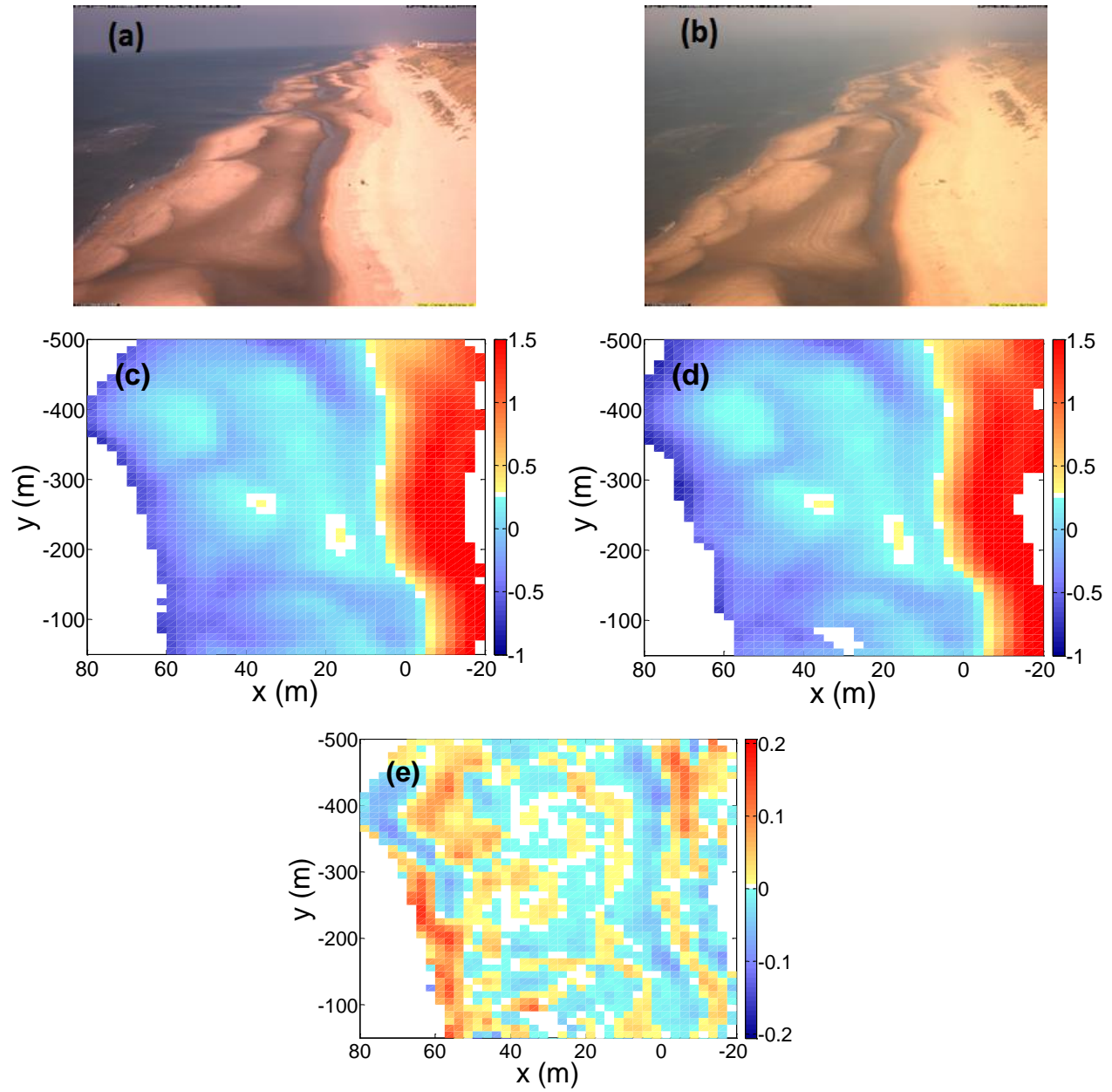


Figure 9. Argus video images at the (a) start of the first period on day 1 and (b) at the end of the period on day 4 with the corresponding DEM's at the (c) start and (d) end of the period and the (e) Difference Model.

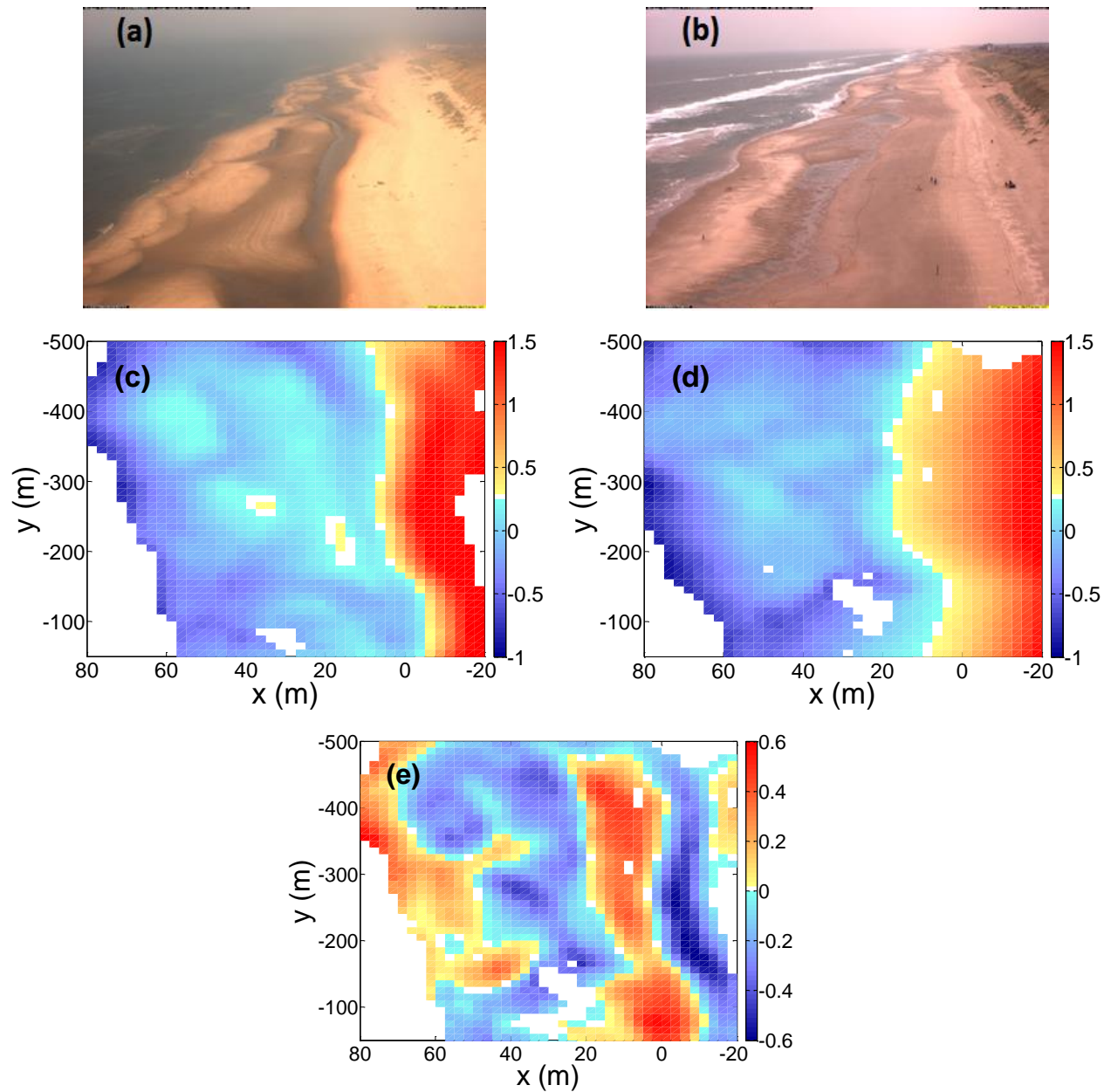


Figure 10. Argus video images at the (a) start of the second period on day 4 and (b) at the end of the period on day 11 with the corresponding DEM's at the (c) start and (d) end of the period and the (e) Difference Model.

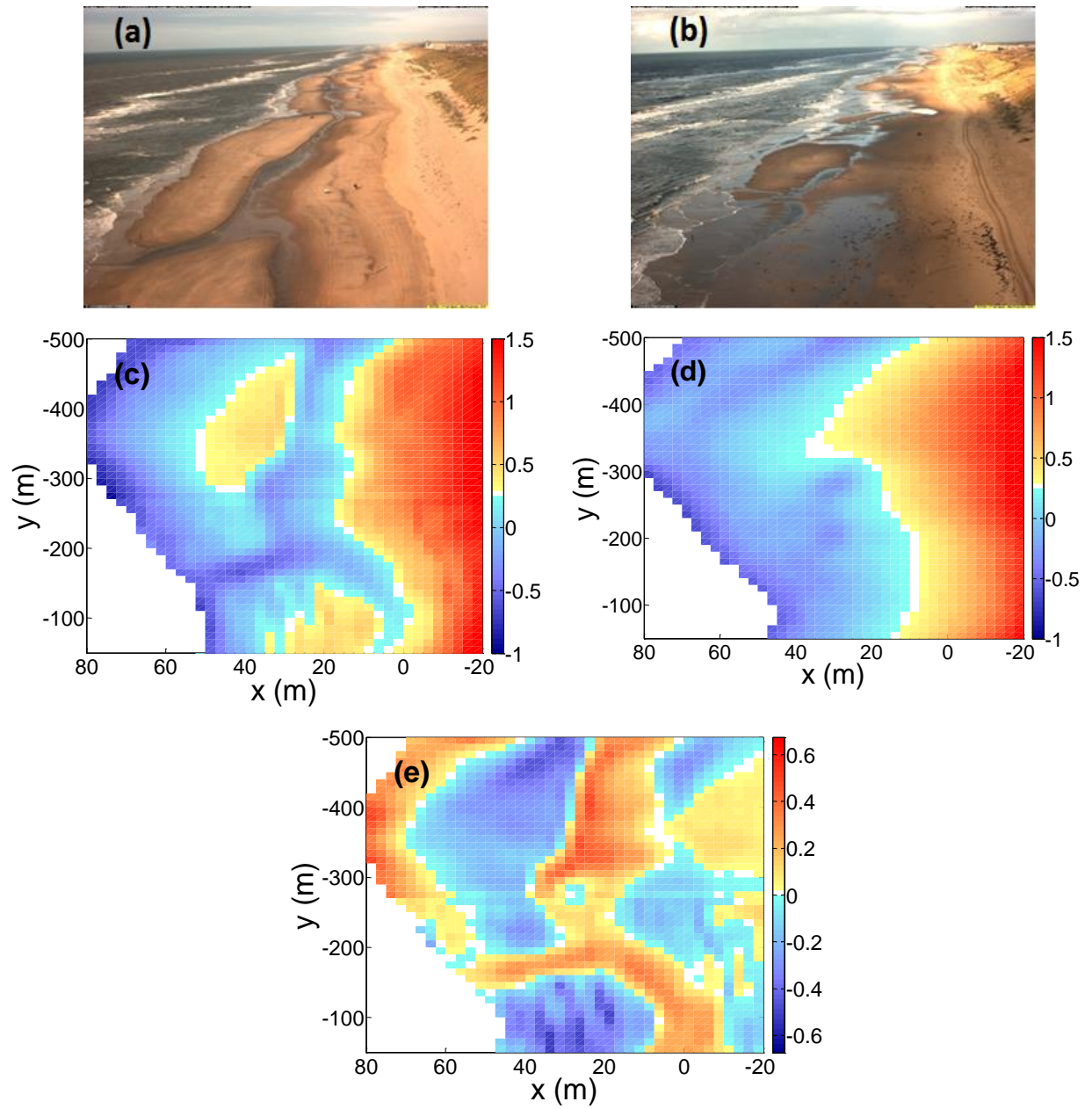


Figure 11. Argus video images at the (a) start of the third period on day 19 and (b) at the end of the period on day 22 with the corresponding DEM's at the (c) start and (d) end of the period and the e) Difference Model.

3 METHODOLOGY

To determine the spatial variability of the morphology, the morphodynamic zone distribution and the changes in morphology, the alongshore uniformity is tested using the approach of Plant et al. (1999) (section 3.1). Section 3.1 describes the model that is used to determine the morphodynamic zone distributions. Finally, the accuracy of the model will be tested in section 3.3.

3.1 ALONGSHORE UNIFORMITY

The alongshore uniformity was tested for the Digital Elevation Models (DEM), the Difference Models (DM), and the morphodynamic zone distributions to determine the spatial variability, following the approach of Plant et al. (1999). Below, the approach is explained for the DEMs but the main approach was similar for the DMs and morphodynamic zone distributions.

The main shape of the intertidal beach at Egmond aan zee was more or less concave. Determining the alongshore uniformity of the different DEMs would therefore result in almost similar alongshore uniformities due to the strong alongshore uniformity in the overall shape. However, for this research the spatial variability of the morphological features (i.e. the berm, bar and trough) are of interest. The overall concave shape of the beach was therefore subtracted from the original DEM data to reveal the features of interest, as is described below.

The elevation data of each DEM, $Z(x, y)$, was divided into an alongshore averaged beach elevation, $\bar{Z}_y(x)$, and deviations from the mean, $Z'(x, y)$:

$$Z'(x, y) = Z(x, y) - \bar{Z}_y(x). \quad (2)$$

The alongshore averaged profile was calculated by:

$$\bar{Z}_y(x) = \sum_{j=1}^{N_y} [Z(x, y)] / N_y, \quad (3)$$

where N_y represents the number of grid lines in the alongshore direction. The alongshore averaged profiles were only calculated for cross-shore locations where more than 50% of the alongshore observations were available. These alongshore averaged profiles contained the overall beach shape and morphological features like the berm, bar and trough. By using the Loess method described in section 2.2, the overall beach shape was removed from the alongshore averaged profiles. These smoothed profiles were used as the alongshore averaged profile data, $\bar{Z}_y(x)$, to ensure that the berm, bar and trough features were visible in the $Z'(x, y)$ data. To illustrate the applied method the alongshore averaged profile, the smoothed profile $\bar{Z}_y(x)$ and the corresponding deviation map $Z'(x, y)$ of Period 1 are shown in Figure 12. The results of this method will be provided and discussed in section 4.

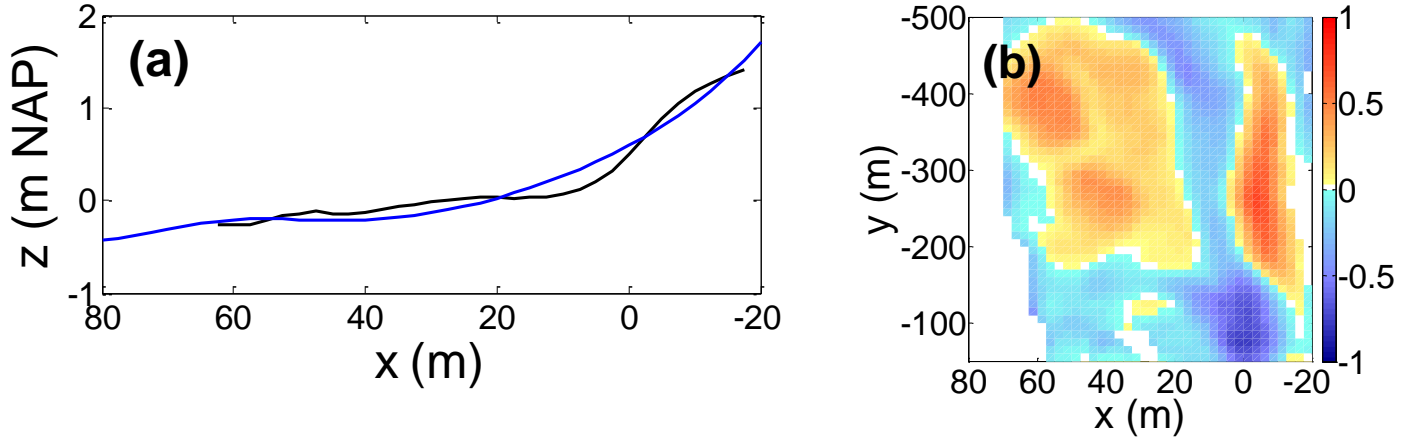


Figure 12. An example of the (a) alongshore averaged DEM (black line) and the smoothed profile (blue) obtained by the Quadratic Loess method. An example of the deviation map is shown in figure b.

The total variance S^2 of the intertidal topography was estimated as the mean-square deviation of $Z'(x, y)$, averaged in both cross-shore and alongshore direction:

$$S^2 = \sum_{j=1}^{N_x} \sum_{i=1}^{N_y} \frac{[Z'(x, y)]^2}{N_x N_y}. \quad (4)$$

By alongshore averaging $Z'(x, y)$ the alongshore-uniform component, $Z'_y(x)$, was calculated as:

$$Z'_y(x) = \sum_{i=1}^{N_y} Z'(x, y) / N_y. \quad (5)$$

The two-dimensional variance s^2 was then calculated as the mean-square deviation of $Z'_y(x)$:

$$s^2 = \sum_{j=1}^{N_x} [Z'_y(x)]^2 / N_x. \quad (6)$$

The fraction of the total variance that was alongshore uniform was obtained by the ratio of s^2 to S^2 . In the extreme potential case of entirely cross-shore uniform $Z'(x, y)$ data, the two-dimensional variance equals the total variance and thus the ratio s^2 and S^2 is 1. In the contrary case with no alongshore uniformity and zero two-dimensional variance the s^2 to S^2 ratio equals zero.

The fraction of the total variance that was alongshore uniform was also calculated for the Difference Models and the morphodynamic zone distributions. Now the approach of Plant et al. (1999) was applied on the original data set $Z(x, y)$ instead of using the deviation data $Z'(x, y)$, since the Difference Models and the morphodynamic zones already show the features of interest and no trend had to be removed.

3.2 MORPHODYNAMIC ZONES

A cross-shore wave transformation model coupled to an inner surf zone model was used to determine the wave propagation across the intertidal beach (section 3.2.1). The main outputs of the model were the wave height, H_{m0} (m), the water depth, $h(m)$, and the wavelength, $L(m)$. With these outputs, the morphodynamic zone boundaries were derived (section 3.2.2). Finally, the model inputs and settings will be described in section 3.2.3.

3.2.1 THE CROSS-SHORE WAVE TRANSFORMATION MODEL COUPLED TO AN INNER SURF ZONE MODEL

The cross-shore wave transformation model is based upon three standard coupled formulations for the cross-shore transformation of organized wave energy (8), the energy of the surface roller (10) and of the mean sea surface elevation (12) also known as the set-up and set-down (Price & Ruessink, 2008). The wave height is derived from the energy density per unit area of a regular sinusoidal wave, which depends on the water density, ρ (kg/m^3) the gravity acceleration, g (m/s^2) and the wave height, H (m):

$$E = \frac{1}{8} \rho g H^2. \quad (7)$$

Assuming alongshore-uniform bathymetry and stationary wave conditions the energy flux balance (organized wave theory) is represented by:

$$\frac{\partial}{\partial x} (E c_g \cos \theta) + D_{br} + D_{bf} = 0. \quad (8)$$

Here, c_g (m/s) is the wave group velocity, ϑ ($^\circ$) is the angle of the waves with respect to the shore normal and x is the horizontal coordinate perpendicular to the shoreline with positive values directed onshore. D_{br} and D_{bf} represent the energy dissipation due to wave breaking and bottom friction. The breaking-induced energy dissipation D_{br} is given by Battjes and Janssen (1978):

$$D_{br} = \frac{1}{4} Q_b \rho g \frac{1}{T_p} H_m^2, \quad (9)$$

where T_p (s) is the wave spectrum peak period, Q_b (-) the fraction of breaking waves and H_m (m) the maximum wave height. The energy dissipation by bed friction (8) is considered relatively unimportant inside the surf zone (Aarninkhof & Roelvink, 1999) and will not be further discussed. After waves break their wave energy is partly converted into the creation of a foamy wave roller. This roller influences the wave energy balance and is given by (Stive & De Vriend, 1994):

$$\frac{\partial}{\partial x} (2E_r c \cos \theta) = -D_r + D_{br}, \quad (10)$$

where E_r (J) is the roller energy density, c (m/s) the phase velocity, D_{br} is the energy dissipation by breaking as computed from equation (9). D_r is the roller dissipation modeled as (Duncan, 1981 and Deigaard, 1993):

$$D_r = \frac{2gE_r \sin \beta}{c}, \quad (11)$$

with θ representing the wave front slope. The energy balance equations can be solved in the onshore direction by a simple forward stepping scheme for given bathymetry and offshore values of H_{rms} , T , θ and tide level. The wavelength, L (m), follows from linear wave theory.

Finally, the wave set-up, η (m), was determined from the depth-integrated and time-averaged cross-shore momentum balance equation, given by:

$$\frac{dS_{xx}}{dx} + \rho gh \frac{d\bar{\eta}}{dx} = 0. \quad (12)$$

The water depth $h(m)$ at a given point on the beach profile can be calculated by:

$$h = \zeta + \eta - z, \quad (13)$$

where ζ (m) is the water level with respect to N.A.P. (Normal Amsterdam Level), η (m) is the set-up/ set-down and z (m) is the bed level with respect to N.A.P. Both water level and bed level are inputs of the model.

The cross-shore momentum flux (S_{xx}) for normally incident wave (also referred to as radiation stress) is given by the linear wave theory as:

$$S_{xx} = \left(\frac{1}{2} + \frac{2kh}{\sinh 2kh} \right) E. \quad (14)$$

Here, k ($2\pi/L$) is the wave number and h (m) the water depth. The wave transformation model is known to fail in shallow water, where the actual wave height exceeds the predicted wave height due to a lack of dissipation mechanisms (Battjes & Janssen, 1978). Therefore, the cross-shore wave transformation model is run until the normalized wave period exceeded 20 for the first time (Price & Ruessink, 2008). The normalized wave period is defined as:

$$T_{nl} = T_{m02} \sqrt{g/h}. \quad (15)$$

With a peak period of 5 seconds, the shoreward end of the wave transformation model is set to a water depth of 60cm. The output of the cross-shore wave transformation model at this point is used as input for the Inner Surf zone Model, ISM (Aarninkhof & Roelvink, 1999) which is more accurate in shallow water. The maximum run-up height, which is also the landward boundary of the swash zone, is computed by the ISM at a water depth of zero ($h = 0$ m). By combining the output of the cross-shore wave transformation model and the ISM, it is possible to derive the morphodynamic zone distribution over the beach profile for a given period.

3.2.2 THE MORPHODYNAMIC BOUNDARIES

In order to determine if the observed intertidal beach changes were caused by cross-shore processes, the morphodynamic zone distribution was calculated for each period. The boundaries of the morphodynamic zones were defined by Price and Ruessink (2008). They found a linear relation between the relative wave height (H_{m0}/h) and the local wave steepness (H_{m0}/L) on the transition between the shoaling wave zone and the surf zone, as well as for the transition between the surf zone and the swash zone (Figure 13). The wavelength, L (m), was taken as the shallow-water wavelength:

$$L = T_{m01}\sqrt{gh}, \quad (16)$$

where $T_{m01}(s)$ is the reciprocal of the centroid frequency (Price & Ruessink, 2008), $g(m/s^2)$ is the gravitational acceleration and h (m) is the water depth (13).

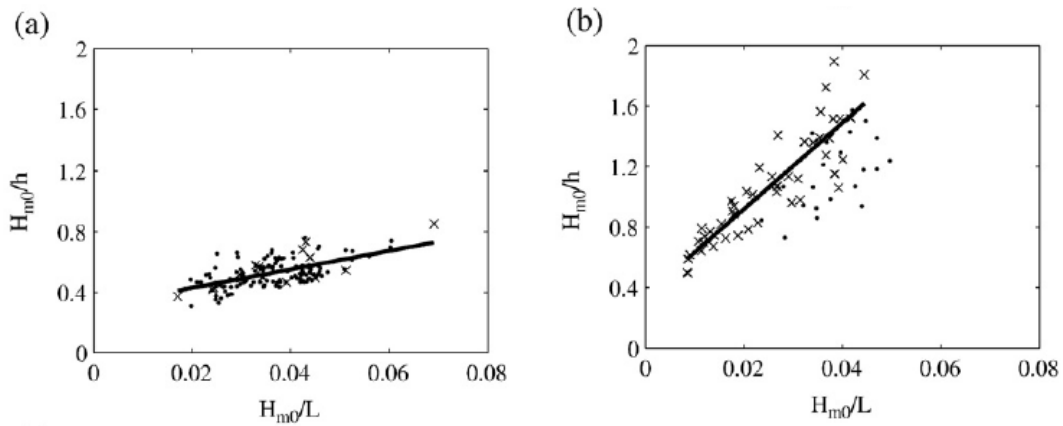


Figure 13. The relative wave height H_{m0}/h versus the local wave steepness H_{m0}/L at the transition of the shoaling zone and the surf zone (a), and the lower end of the swash zone (b). The dots are video-derived estimates and the crosses are derived from in situ measurements. The lines are the best linear fits given by equation (17) and (18). (Price & Ruessink, 2008).

The best linear fit for the transition from the shoaling wave zone to the surf zone is given by (Figure 13a):

$$\left[\frac{H_{m0}}{h} \right]_b = 6.1 \frac{H_{m0}}{L} + 0.31. \quad (17)$$

The subscript b indicates the breakpoint. For the transition between the surf zone and the lower end of the swash zone, the following linear relation exists (Figure 13b):

$$\left[\frac{H_{m0}}{h} \right]_s = 29 \frac{H_{m0}}{L} + 35. \quad (18)$$

Here, the subscript s indicates the lower end of the swash zone. Consequently, the surf zone is given by:

$$6.1 \frac{H_{m0}}{L} + 0.31 \leq \frac{H_{m0}}{h} < 29 \frac{H_{m0}}{L} + 0.35. \quad (19)$$

3.2.3 MODEL IMPLEMENTATION

The cross-shore wave transformation model coupled to an inner surf zone model was run for the three selected periods (Table 2). The input of the model consisted of offshore wave and tide conditions (wave height, wave period, angle of wave incidence relative to shore-normal and water level, Figure 7) and beach profile data. The profile data originated from the digital elevation models. Each DEM was divided into 46 cross-shore profiles spaced 10m and missing data was repaired by linear interpolation. The cross-shore profiles were all extended landward with the measured fore dune profile (Figure 5) and seaward with offshore bathymetry obtained by Rijkswaterstaat. Each location of the 46 cross-shore profiles had one specific offshore profile which remained constant through time. The cross-shore profiles were interpolated over a cross-shore x-axis with variable intervals. The interval of the x-axis was relatively large offshore due to the relatively constant bathymetry, and decreased shoreward where the variability in morphology increased. The profiles were also linearly interpolated between the observations, with a time interval of 15 minutes.

The model used some free parameters to calculate the different energy dissipations. The dissipation due to wave breaking was calculated using the proportionality coefficient, $\alpha(-)$, here set to 1. The dissipation due to bed friction was determined with a friction coefficient that was described by the wave related roughness ($ks = 0.025m$). Furthermore, the slope of the wave front ($\beta(-) = 0.1$) was used in the roller dissipation and finally the breaker parameter $\gamma(-)$ determined the dissipation rate due to depth induced wave-breakers and was fixed at 0.74.

The output of the model runs were the modeled wave properties and the relative occurrence of the morphodynamic zones, both calculated for each profile at each cross-shore position for each time step. The relative occurrence of the morphodynamic zones is the percentage of time that a certain zone was active with respect to the total time that the location was submerged. The morphodynamic zone distribution of all the cross-shore profiles was used to create an interpolated map for each morphodynamic zone.

3.3 ACCURACY ANALYSIS

In this section, the modeled wave height is compared with the measured wave height to determine the accuracy of the model and therefore the reliability of the morphodynamic zone distributions.

During the field campaign, thirteen pressure sensors (indicated by P1 to P13) were aligned in a cross-shore transect at the center of the fieldwork area (Table 3) to determine the wave height. The pressure sensors collected data with a frequency of 4Hz or 5Hz and the height of the instruments above the bed was measured daily and adjusted when needed. The sensors were kept at a height of 0-20 cm above the bed and the values between the measurements were linearly interpolated. Measured pressure signals were corrected for air pressure measured by a local device, and converted into water elevation above the sensor. The elevation was then converted with linear wave theory to sea surface elevation. The water depths, $h(m)$, were calculated as the mean of the measured elevation plus the instrument height. Finally, the pressure data was processed in bursts of 15 minutes and wave energy spectra $E(f)$, a function of frequency (f), were calculated for time-series with a length of 15 minutes, Hanning window blocks and 50% overlap. The wave heights were calculated as

$$H_{m0} = 4\sqrt{(m_0HF)}, \quad (20)$$

with m_0HF as the zeroth moment of the energy spectra for high frequency waves. The high frequency (HF) and low frequency (LF) wave heights were taken as the zeroth moment for the spectrum with HF $0.05 < f < 1\text{Hz}$ and $LF < 0.05\text{Hz}$.

Table 3. The cross-shore location of the thirteen pressure sensors, indicated seaward by P1 to P13.

Pressure Sensor	P1	P2	P3	P4	P5	P6	P7	P8	P9	P10	P11	P12	P13
Location x(m)	-2,5	2,5	6,5	14	25,5	31	39,5	43	49	55	63	70	77

For the three selected periods, the offshore wave height at station ‘Stroommeetpaal IJmond’, the wave height measured by the most seaward pressure sensor (P13) and the modeled wave height at P13 are displayed in Figure 14. The wave height data for Period 2 and 3 showed a tidal signal (Figure 14b and c), because the tide changes the water depth and therefore also the wave height of the breakers, as waves generally break in a water depth of 1.3 times their wave height.

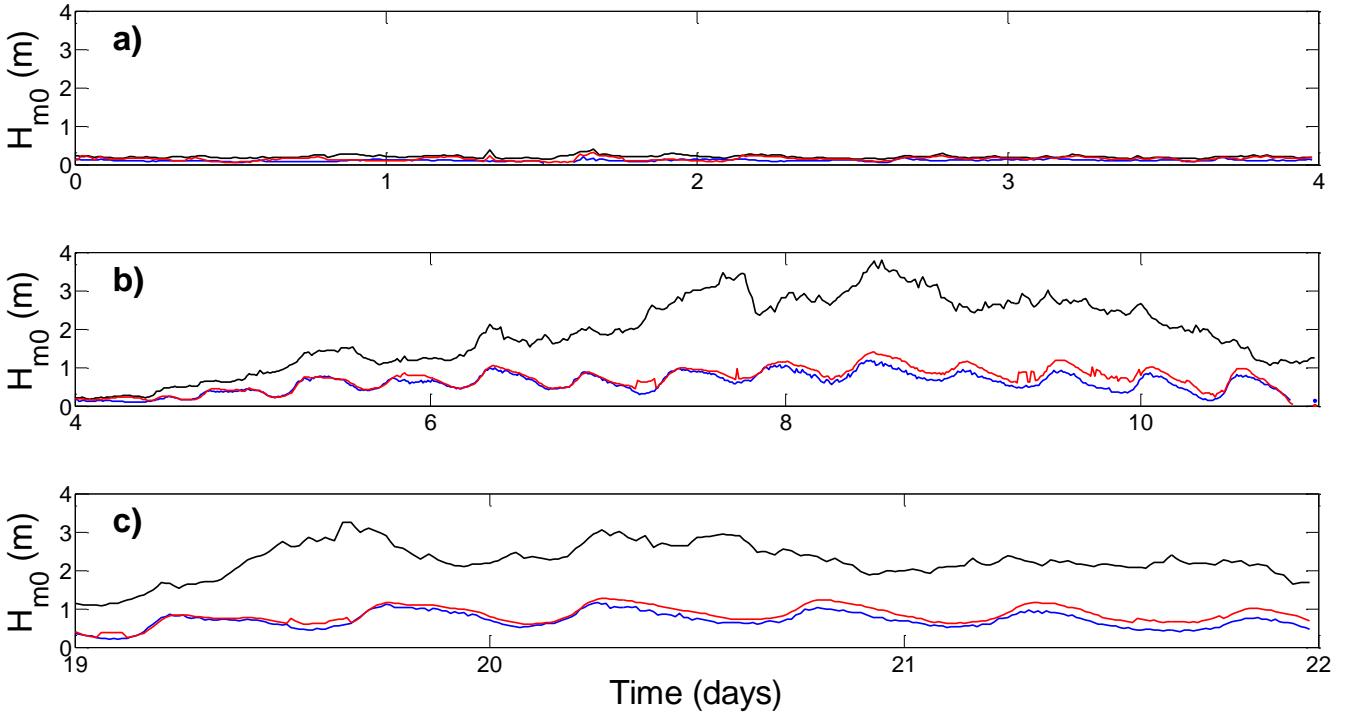


Figure 14. The measured wave height at station 'Stroommeetpaal IJmond' (black line), the measured wave height at the most seaward pressure sensor P13 (blue line) and the modeled wave height at the location of P13 (red line) for the selected periods (a) 1, (b) 2 and (c) 3.

The accuracy of the modeled wave height was assessed by comparing the modeled wave height with the measured wave height. The coefficient of determination, R^2 (-), the root mean square error, $RMSE$ (m), and the slope of the best fit line, m (m/m), were calculated for every pressure sensor location and for all three selected periods (Table 4). Period 1 had the lowest average R^2 and m but also the lowest average $RMSE$ (= 0.08m). Nevertheless, as is stated in section 2.3, the input of the model during Period 1 is not representative for the intertidal beach as offshore directed waves were measured (Figure 7). Period 2 and 3 had both similar statistics with an R^2 around 0.85(-), m of 0.84 m/m and an $RMSE$ of 0.20m. The offset of the model was relatively small as the offshore wave heights were up to 3 to 4 meter. Overall, the model slightly over predicted the wave height during Period 2 and 3 (Table 4) with an increase towards the end. This offset may be caused by changes in offshore morphology that were induced by the high energetic wave conditions and not incorporated in the input of the model.

Table 4. The coefficient of determination, r^2 (-), the root mean square error, RMSE (m), and the slope of the best fit line, m (m/m), for all the pressure sensor locations (P) and for the three selected periods.

P	Period 1			Period 2			Period 3		
	r^2	RMSE	m	r^2	RMSE	m	r^2	RMSE	m
1	0,30	0,13	0,42	0,88	0,16	0,88	0,85	0,18	0,72
2	0,17	0,06	0,46	0,81	0,12	0,81	0,86	0,22	0,78
3	0,52	0,06	0,47	0,88	0,14	0,88	0,87	0,23	0,79
4	0,51	0,09	0,77	0,91	0,22	0,91	0,77	0,25	0,96
5	0,35	0,08	0,63	0,50	0,35	0,50	0,77	0,22	0,82
6	0,13	0,10	0,34	0,45	0,36	0,45	0,82	0,21	0,70
7	0,31	0,08	0,73	0,89	0,16	0,89	0,88	0,17	0,71
8	0,34	0,08	0,59	0,83	0,17	0,83	0,94	0,15	0,79
9	0,35	0,06	0,44	0,92	0,14	0,92	0,93	0,16	0,85
10	0,25	0,07	0,46	0,94	0,15	0,94	0,91	0,18	0,91
11	0,17	0,11	0,52	0,85	0,33	0,85	0,90	0,31	1,40
12	0,11	0,06	0,20	0,91	0,17	0,91	0,93	0,14	0,76
13	0,12	0,06	0,19	0,87	0,15	0,87	0,87	0,15	0,86
Average	0,28	0,08	0,48	0,82	0,20	0,82	0,87	0,20	0,85

The accuracy of the model was also investigated in cross-shore direction (Figure 15). Pressure sensors 5 and 6 showed both a notable deviation in RMSE and R^2 for Period 2 and 3. Pressure sensor 11 also had an aberration as it was the only pressure sensor that had a best fit slope larger than 1 m/m ($m = 1.40$ m/m) during Period 3. In addition, pressure sensor 11 showed a deviation in RMSE during Period 2 and 3 similar to pressure sensor 5 and 6.

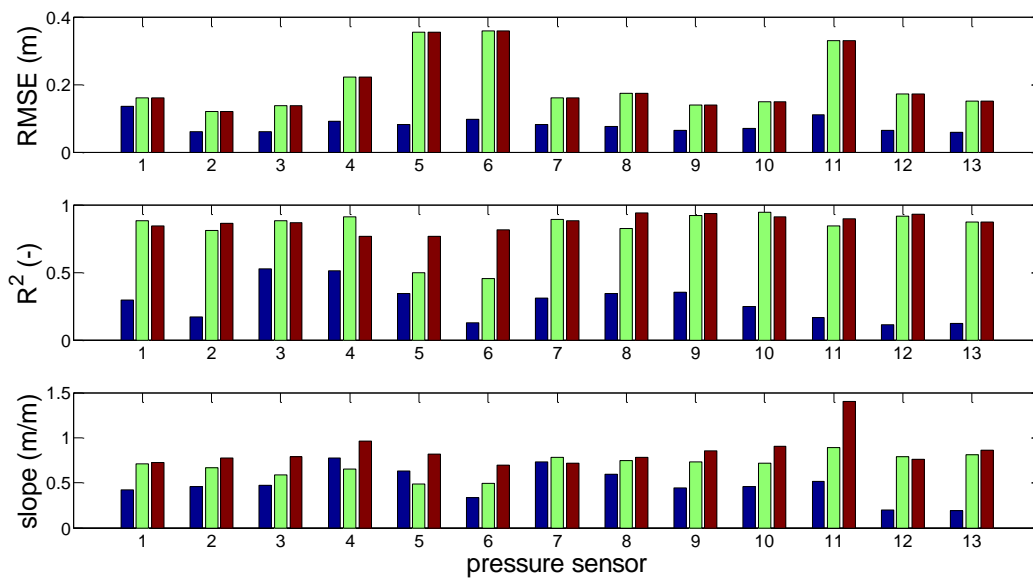


Figure 15. The root mean square error, RMSE (m), coefficient of determination, R^2 (-), and the slope of the best fit line, m (m/m), along the pressure sensors for Period 1 (blue), Period 2 (green) and Period 3 (red).

Figure 16 displays the modeled wave heights against the measured wave heights of pressure sensor 5, 6 and 11 during Period 2. Fortunately, a survey was made between the first and the last day of Period 2 (at day 7) helping to track the evolution of the beach profile during Period 2 in more detail (Figure 16d). The beach profile data used as input for the model was linear interpolated between the first and the last day of the period and resulted in erosion for the locations of pressure sensor 5 and 6. However, the beach profile at day 7 showed accretion at pressure sensor 5 and 6. This increase in elevation would result in a decreased water and wave height, but the linear interpolated elevation data showed an increased water height and related wave height. Figure 16b and c display this offset by a dichotomy in the data set. Unfortunately, the survey at day 7 does not include the location of pressure sensor 11 due to high water levels. The modeled and measured wave height data for pressure sensor 11 (Figure 16a) show a relatively large scatter around the low measured wave heights, which implies that the water level was actually lower than the interpolated water level. Unfortunately the beach was not surveyed between the first and the last day of Period 3, complicating the explanation behind the observed deviations during this period. Concluding, the assumption that morphology changes linearly over time has shown to be incorrect and resulting errors do influence the results and accuracy of the model. Frequent profile measurements within a period will improve model performance.

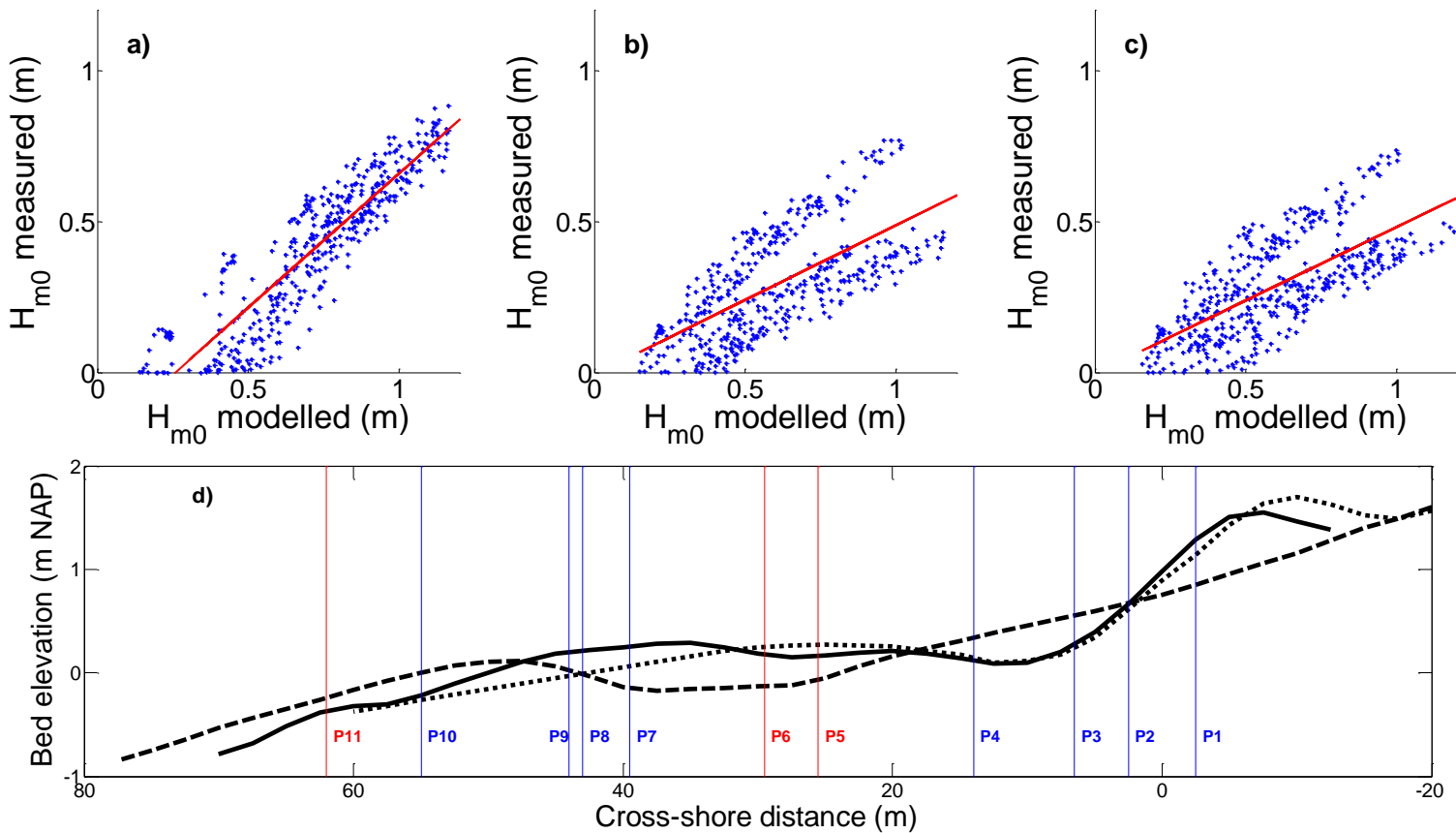


Figure 16. The measured H_{m0} and modeled H_{m0} for (a) pressure sensor 11 (P11), (b) pressure sensor 6 (P6), pressure sensor 5 (P5) and the best fit line (red line) during Period 2. The intertidal beach profiles (d) at day 4 (the beginning of Period 2, solid line), day 7 (dashed line) and day 11 (end of Period 2, striped line) with the locations of the pressure sensors.

4 RESULTS

This section presents the results of this research and discusses the process and related factors. The results of the alongshore uniformity of the Digital Elevations Models, DEMs, and Difference Models, DMs, are presented in section 4.1. In section 4.2 the morphodynamic zone distribution is compared with the observed changes in morphology and this is discussed in more detail in section 4.3. Finally, section 4.4 focusses on the alongshore variability of the intensity of morphodynamic zone processes.

4.1 SPATIAL VARIABILITY OF THE DIGITAL ELEVATION AND DIFFERENCE MODELS

In order to answer the second sub-question of this research (section 1: *Are the observed changes in intertidal beach morphology two- or three-dimensional?*) the approach of Plant et al. (1999) was used (section 3.1) to determine the spatial variability of the DEMs and DMs. Section 4.1.1 will present the intermediate results of the approach used by Plant et al. (1999) applied on the DEMs and section 4.1.2 will present and discusses the alongshore uniformity results of both the DEMs and DMs.

The main morphological changes during the three periods are discussed in detail in section 2.4. In short, the beach face steepened and the intertidal bar slightly increased and migrated onshore during the low energetic wave conditions of Period 1. Period 2 and 3 were characterized by high energetic wave conditions, causing an overall smoothing of the morphology. During both periods the beach face eroded and became less steep and the intertidal bar flattened and migrated offshore. Low laying morphological features like the trough and rip channel faded and the southern rip channel even disappeared in Period 3.

4.1.1 THE PERTURBATIONS OF INTEREST OF THE DIGITAL ELEVATION MODELS

In order to determine the alongshore uniformity of the Digital Elevation Models and Difference Models, the fraction of the total variation that is alongshore uniform was determined using the approach of Plant et al. (1999). As described in more detail in section 3.1, the deviations from the DEMs were used to calculate the total variation and the two-dimensional variation for the intertidal beach morphology. These deviations were obtained by subtracting the alongshore averaged data set from the original data set (2). To determine the alongshore uniformity of the DEMs, a smoothed beach profile was used as a substitute for the alongshore averaged profile in order to preserve the features of interests, such as the berm, bar and trough, in the deviation data.

The alongshore averaged DEMs and the smoothed profiles at the beginning and end of the three periods are shown in Figure 17. Figure 18 displays the deviations from the smoothed profiles that were obtained by subtracting a smoothed profile from the original DEM revealing the berm, bar and trough features. The deviation in the morphology of Period 1 (Figure 17a & Figure 17b and Figure 18a & Figure 18b) and in the beginning of Period 2 (Figure 17c and Figure 18c) show a developed morphological pattern with, in the southern part, a clear berm, trough, bar and a rip channel. The intertidal bar and trough are still present after the first period with high energetic wave conditions, but less developed and more offshore located (Figure 17d and Figure 18d). The berm disappeared during this storm event and the beach face shows an alongshore variation in height, where the beach face between $y = -450\text{m}$ and $y = -200\text{m}$ is relatively high compared to the rest of the beach face. This elevated part of the beach face corresponds to the widest part of the beach face (Figure 10d). The beginning of Period 3 also shows this alongshore beach face variation together with two intertidal bars, separated by a rip channel, and a trough (Figure 18e and Figure 11c). The morphological features at the beginning of Period 3 are less developed compared to the initial morphology of Period 1 and 2 (Figure 17e). The high energetic wave conditions during Period 3 result in an overall smooth beach profile of which the alongshore averaged profile is almost equal to the calculated smoothed profile (Figure 17f). The deviations at the end of Period 3 (Figure 18f) are divided cross-shore into a relatively low laying area in the south, between $y = -50\text{m}$ and $y = -250\text{m}$, and a relatively high area

in the north, between $y = -250\text{m}$ and $y = -500\text{m}$. As this pattern is not common for morphological features, this offset is most likely the result of measurement errors that were not corrected properly (section 2.2).

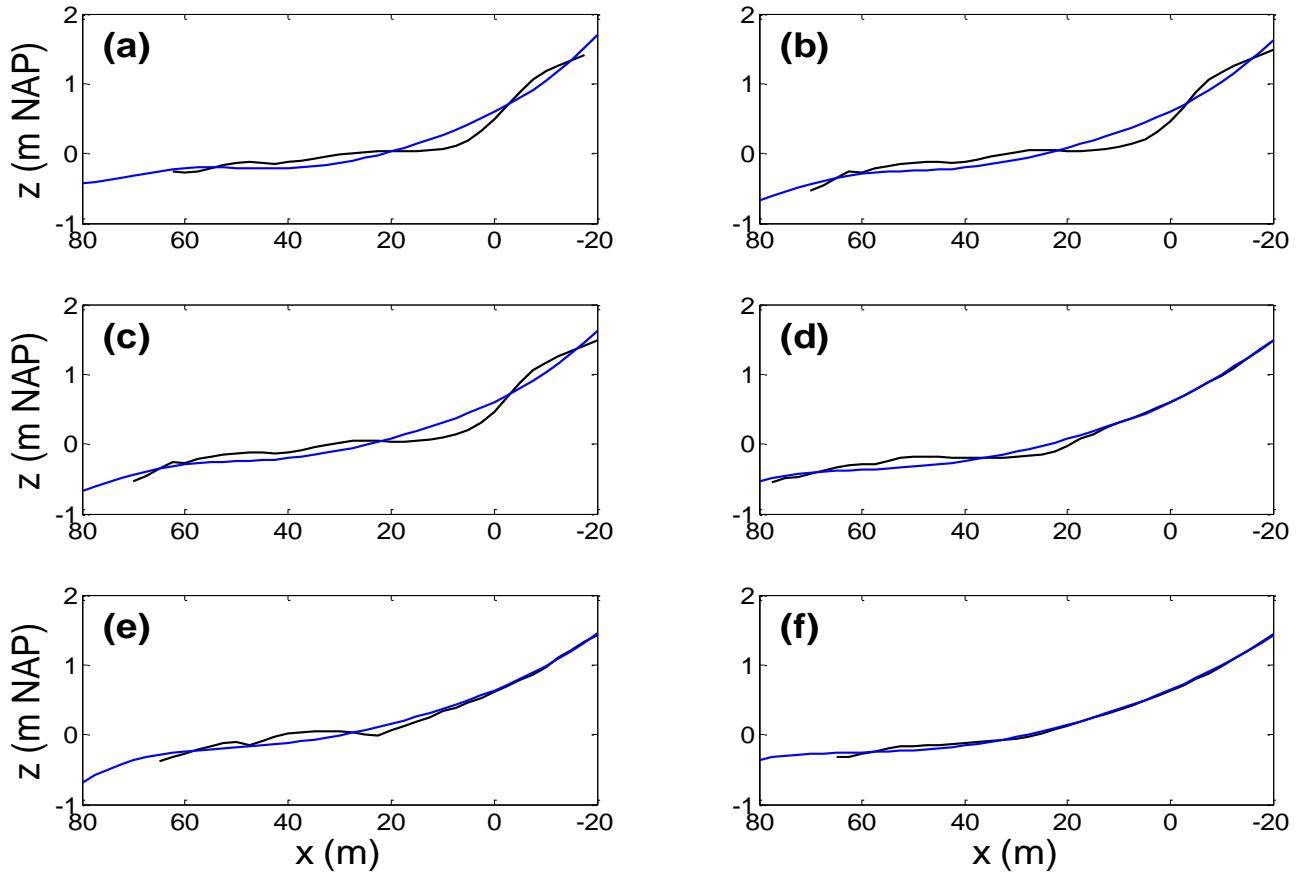


Figure 17. The alongshore averaged profiles (black line) and smoothed profiles (blue line) of the beginning (a) and end (b) of Period 1, beginning (c) and end (d) of Period 2 and the beginning (e) and end (f) of Period 3.

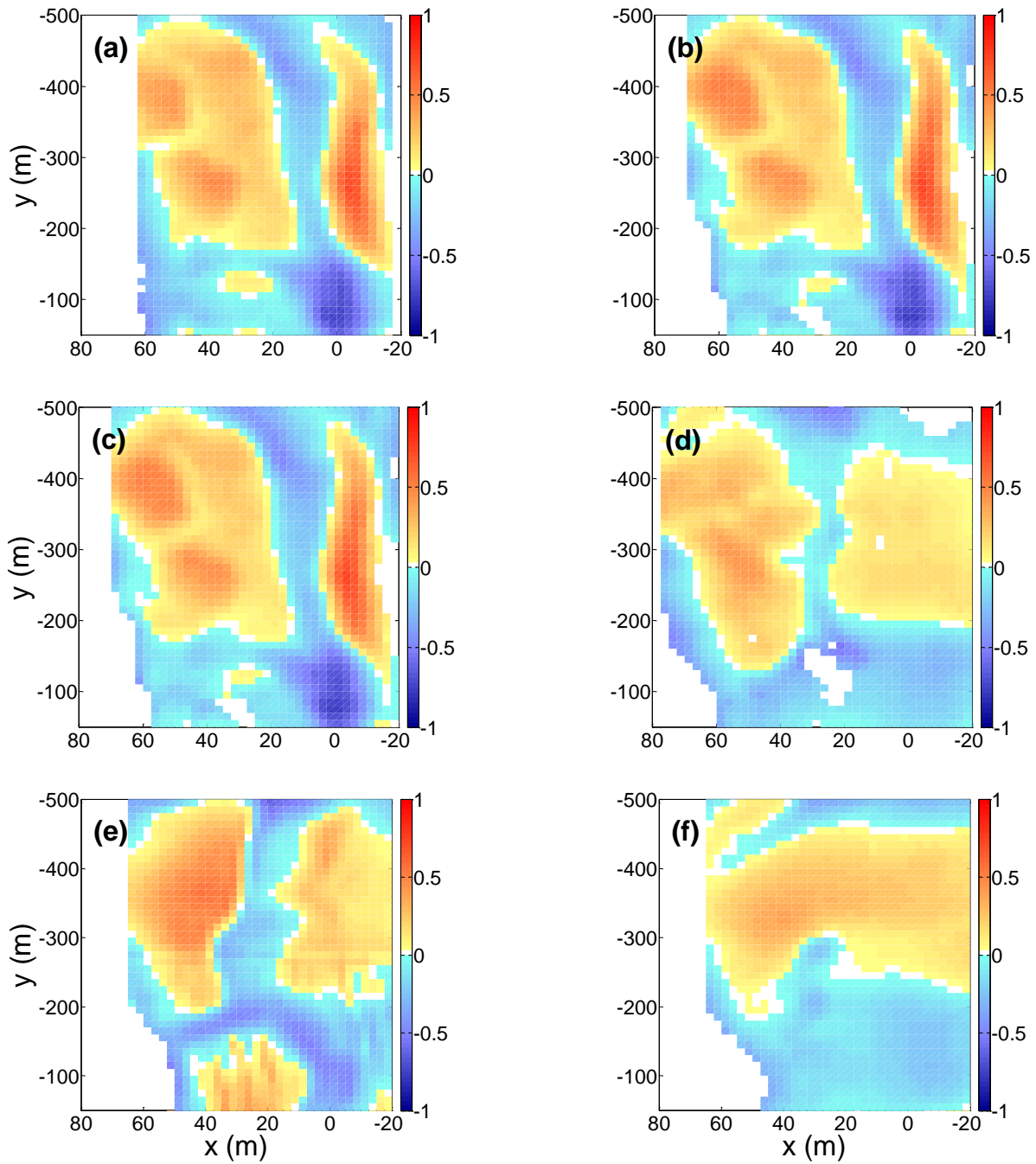


Figure 18. The deviation maps of the beginning (a) and end (b) of Period 1, beginning (c) and end (d) of Period 2 and the beginning (e) and end (f) of Period 3.

4.1.2 ALONGSHORE UNIFORMITY

The total variance, the two-dimensional variance and the fraction of the total variance that is alongshore uniform is determined for the Digital Elevations Models and the corresponding Difference Models of each period (Table 5). This allows comparison of the alongshore uniformity of the DEMs at the beginning and end of each period to determine if the morphology turned more alongshore uniform (increased alongshore uniformity) or more alongshore variable (decreased alongshore uniformity) during that specific period.

During Period 1, the alongshore uniformity of the DEMs changes from $s^2/S^2 = 0.18$ at the beginning to $s^2/S^2 = 0.21$ at the end. This indicates that the morphology became more alongshore uniform during this period with low energetic wave conditions. Compared to the other fractions, the alongshore uniformity is the highest at the end of Period 1 (Table 5) when also the total variance and two-dimensional variance reach their highest values. This indicates that the well-developed berm, bar and trough features (Figure 17b and Figure 18b) do cause alongshore variation in intertidal morphology. However, their main pattern is shore parallel and induce, therefore, an increase in alongshore uniformity. The changes in intertidal beach morphology during Period 1 are relatively small, with a total variance of $S^2 = 0.0014\text{m}^2$ and a two-dimensional variance of $s^2 = 0.0003\text{m}^2$, which results in an alongshore uniformity of $s^2/S^2 = 0.2150$.

The high energetic wave conditions of Period 2 cause a decrease in both the total variance (from $S^2 = 0.070\text{m}^2$ to $S^2 = 0.034\text{m}^2$) and the two-dimensional variance (from $s^2 = 0.015\text{m}^2$ to $s^2 = 0.004\text{m}^2$). The two-dimensional variance reduces significantly more than the total variance, which results in a decrease of the alongshore-uniform variance fraction from $s^2/S^2 = 0.21$ to $s^2/S^2 = 0.13$. During Period 2, the intertidal beach changes have an alongshore uniform fraction of $s^2/S^2 = 0.397$. This is, compared to the other fractions of the difference maps, the biggest alongshore uniform intertidal beach change observed.

The total variance at the beginning of Period 3 ($S^2 = 0.072\text{m}^2$) is almost equal to the total variance at the beginning of Period 1 and 2 but the two-dimensional variance is significantly lower ($s^2 = 0.005\text{m}^2$) causing the fraction of alongshore variance to be relatively small, $s^2/S^2 = 0.064$. The morphology slightly amplified between Period 2 and 3 (Figure 17d and Figure 17e) which results in an increase of the two-dimensional variance of $s^2 = 0.004\text{m}^2$ to $s^2 = 0.005\text{m}^2$ respectively. Similar to Period 2, the high energetic wave conditions during Period 3 cause a decrease in total variance (from $S^2 = 0.72\text{m}^2$ to $S^2 = 0.037\text{m}^2$) and two-dimensional variance (from $s^2 = 0.005\text{m}^2$ to $s^2 = 0.002\text{m}^2$). This results in an alongshore uniform variance fraction of $s^2/S^2 = 0.056$. The fraction of the alongshore variance of the DM of Period 3 is relatively low, with $s^2/S^2 = 0.090$.

The morphology of the intertidal beach responded differently on the two high energetic wave conditions of Period 2 and 3. Even though both storms induced offshore bar migration and flattening of the entire morphology, the high energetic wave conditions during Period 3 also led to the disappearance of a rip channel (section 2.4). In addition, the observed changes in morphology during Period 3 were relatively more alongshore variable, with $s^2/S^2 = 0.090$, compared to Period 2, with $s^2/S^2 = 0.397$. As described in section 1, the decay of three-dimensional features, to which a rip channel belongs, is induced by strong alongshore currents generated by oblique incident waves. However, the offshore angle of incidence (Figure 7c) was almost identical for Period 2 and 3. It is therefore not possible that the offshore wave conditions are responsible for the different changes in intertidal beach morphology. However, a major difference between Period 2 and Period 3 is the initial beach morphology. Period 2 started with a relatively alongshore uniform and well-developed morphology while the morphology at the beginning of Period 3 was relatively flat and alongshore variable as a result of the high energetic wave conditions during Period 2. These differences in initial morphology may therefore be the cause of a different morphological response.

Table 5. The total variation S^2_{tot} , two-dimensional variation s^2_{2D} and the ratio between s^2_{2D} and S^2_{tot} for the beginning and end of the three periods and for the Difference Models

	Period 1			Period 2			Period 3		
	Begin	End	DM	Begin	End	DM	Begin	End	DM
$S^2_{tot} (m^2)$	0.069	0.070	0.0014	0.070	0.034	0.061	0.072	0.037	0.046
$s^2_{2D} (m^2)$	0.012	0.015	0.0003	0.015	0.004	0.024	0.005	0.002	0.004
s^2_{2D} / S^2_{tot}	0.178	0.212	0.2150	0.212	0.129	0.397	0.064	0.056	0.090

Since the morphology displays a clear coast parallel pattern with well-developed berm, bar and trough features, the fractions of the alongshore uniform variances of the DEM at the beginning and end of Period 1 are unexpectedly low, with $s^2/S^2 = 0.18$ and $s^2/S^2 = 0.21$ respectively. However, these features do show small alongshore variations and it is hypothesized that the alongshore variable beach width may cause the fraction of alongshore uniform variance to be relatively low. Therefore, the alongshore uniformity was tested again on an adjusted DEM at the end of Period 1, where the maximum height of the upper beach face was taken as $x = 0m$ in order to straighten the beach face (Figure 19). The alongshore uniformity increases from $s^2/S^2 = 0.21$ for the original DEM, to $s^2/S^2 = 0.37$ for the adjusted DEM, nearly a doubling in alongshore uniformity. The alongshore uniformity is also determined for a small, relatively alongshore uniform part of the original DEM, between $y = -400m$ and $y = -200m$, omitting the northern and southern rip channel (Figure 20). For this selected area, the fraction of the total variation that is alongshore uniform is $s^2/S^2 = 0.78$. So the alongshore variation in beach width, and the rip channels cause the fraction of the total variance that is alongshore uniform to decrease in such extent that the morphology is defined as alongshore uniform, despite that the main morphological patterns are coast parallel. In addition, the dimensions of the selected area also influence how alongshore uniform the morphology is.

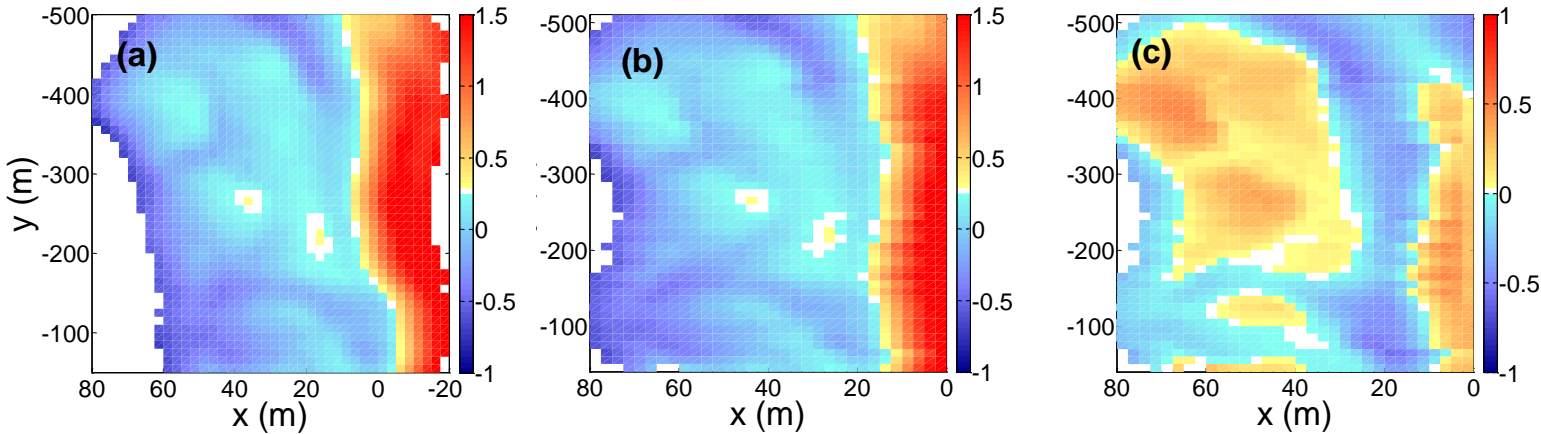


Figure 19. The (a) initial DEM at the end of Period 1, the (b) adjusted DEM with the straightened beach and (c) the deviation map of the adjusted DEM

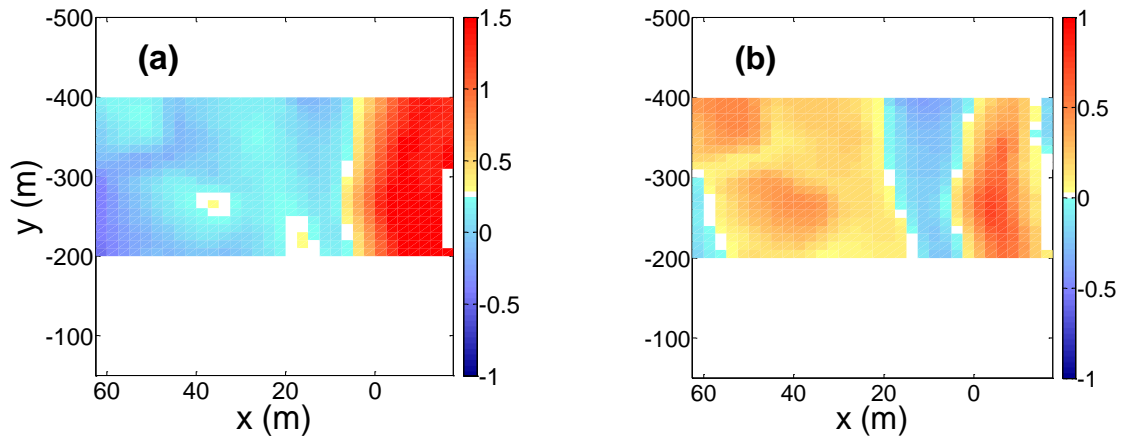


Figure 20. The (a) selected DEM area of the end of Period 2, and (b) corresponding deviation map.

4.2 MORPHODYNAMIC ZONES

The distribution of the relative occurrence of the morphodynamic zones (section 4.2.1) was calculated using a cross-shore wave transformation model coupled to an inner surf zone model (section 3.2). The morphodynamic zone distributions are compared to the observed changes in morphology to determine to what extent the observed changes can be explained by the morphodynamic zone distribution (sub-question 3, section 1). Next, the ratio of the two-dimensional and total variance of each morphodynamic zone distribution is calculated to determine the alongshore uniformity of the morphodynamic zone processes (section 4.1.2). Finally, the relation between the morphodynamic zone distribution and the changes in morphology (section 4.2.1) and the cause of the alongshore variability of the intensity of morphodynamic zone processes (section 4.2.3) are discussed.

4.2.1 DISTRIBUTION

The distribution of the relative occurrence of the morphodynamic zones is determined for the three selected periods (Figure 21, Figure 22 and Figure 23). The relative occurrence is the percentage (%) of time that a certain zone is active with respect to the total time that the location is submerged. To analyze the morphodynamic zone distributions and the corresponding changes in morphology the contour lines of the relative occurrence of the morphodynamic zones are plotted on the Digital Elevation Model and Difference Model that correspond to the beginning of each period.

Period 1 showed a high relative occurrence of shoaling (70% - 80%) in the deeper seaward side of the area, in the rip channels and between relatively high elevated parts of the intertidal bar (Figure 21a and Figure 21b). The relative occurrence of shoaling dropped relatively fast (to ~10%) on the intertidal bar due to the sudden decrease in water depth. The shoaling waves did not cause any significant change in intertidal beach morphology as no clear pattern is visible between the shoaling contour lines and the Difference Model (Figure 21c). The surf zone was mostly active on the intertidal bar (40%) and on the lower beach face (60%) (Figure 21d and Figure 21e). However, visual inspections of the Argus video images showed that the surf zone conditions on the intertidal bar actually corresponded to surf zone bores propagating across the intertidal shoal. The onshore bar migration was, therefore, induced by bore processes whereas the beach face was eroded by surf zone processes (Figure 21f). The swash zone was located on the upper beach face for 80% to 90% of the time (Figure 21g and Figure 21h). The contour lines of the swash zone correspond exactly to the alongshore sedimentation pattern on the upper beach face, indicating that the swash zone transported suspended sediment from the lower beach face to the upper beach face and thereby increasing the beach face slope (Figure 21i).

The high energetic wave conditions during Period 2 caused the intertidal beach to be dominated by surf zone processes (70% - 80%) which induced the offshore bar migration (Figure 22a, Figure 22b and Figure 22c). The swash zone processes were active on a relatively wide part of the intertidal beach face (40% - 80%) and induced erosion (Figure 22d, Figure 22e and Figure 22f). Shoaling waves were active on the seaward side of the intertidal bar, in the low laying areas like the rip channel and in the intertidal trough but the occurrence was, compared to Period 1, relatively low (10% - 40%) (Figure 22g, Figure 22h and Figure 22i).

Period 3 showed a similar morphodynamic zone distribution (Figure 23) as Period 2 (Figure 22) with surf zone processes dominating the intertidal beach (70% - 80%), swash zone processes on the intertidal beach face (40% - 80%) and on both intertidal bars (20%). Shoaling zone processes were active on the seaward side of the area (10% - 40%), in the rip channel and in the intertidal trough (10% - 30%). Overall, the area showed similar changes in intertidal morphology as during Period 2. The intertidal bar flattened and migrated offshore under the prevailing surf zone conditions and the upper beach face partly eroded during swash conditions. However, there are two observed changes in morphology that cannot be explained by the distribution of morphodynamic zones during this period. First of all, the sedimentation of the upper beach face, between $y = -300\text{m}$ and $y = -450\text{m}$ and second, the

sedimentation in the rip channel (around $y = -250\text{m}$) which led to the disappearance of the rip channel. Section 4.3 will further discuss the relation between the disappearance of the rip channel and the morphodynamic zone distribution.

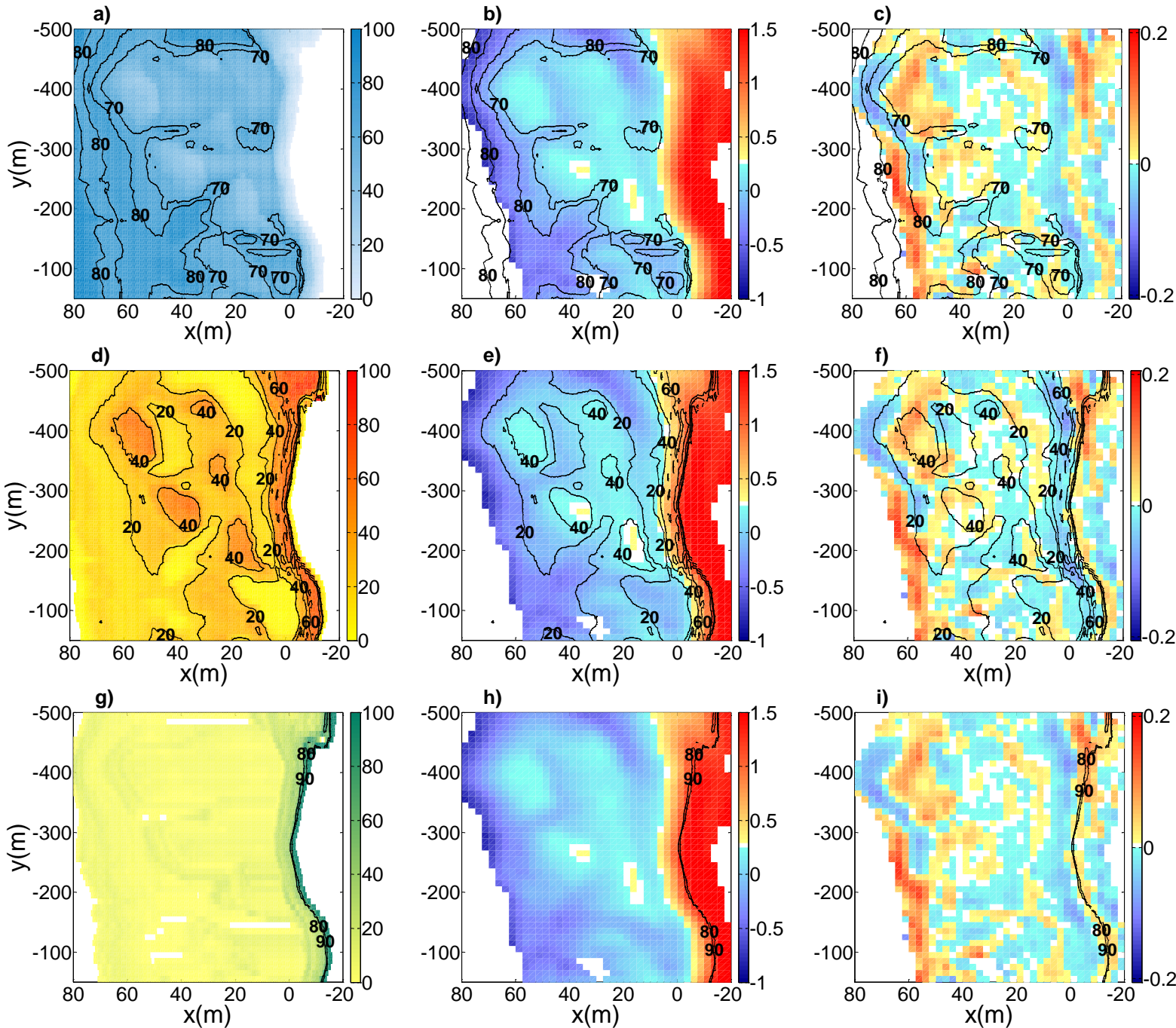


Figure 21. The (a) shoaling zone (blue), (d) surf zone (yellow) and (g) swash zone (green) distribution of Period 1. The contour lines of the (b) shoaling zone, (e) surf zone and (h) swash zone are plotted on the DEM of the beginning of Period 1. In addition, the (c) shoaling, (f) surf and (i) swash contour lines are also plotted on the corresponding Difference Model.

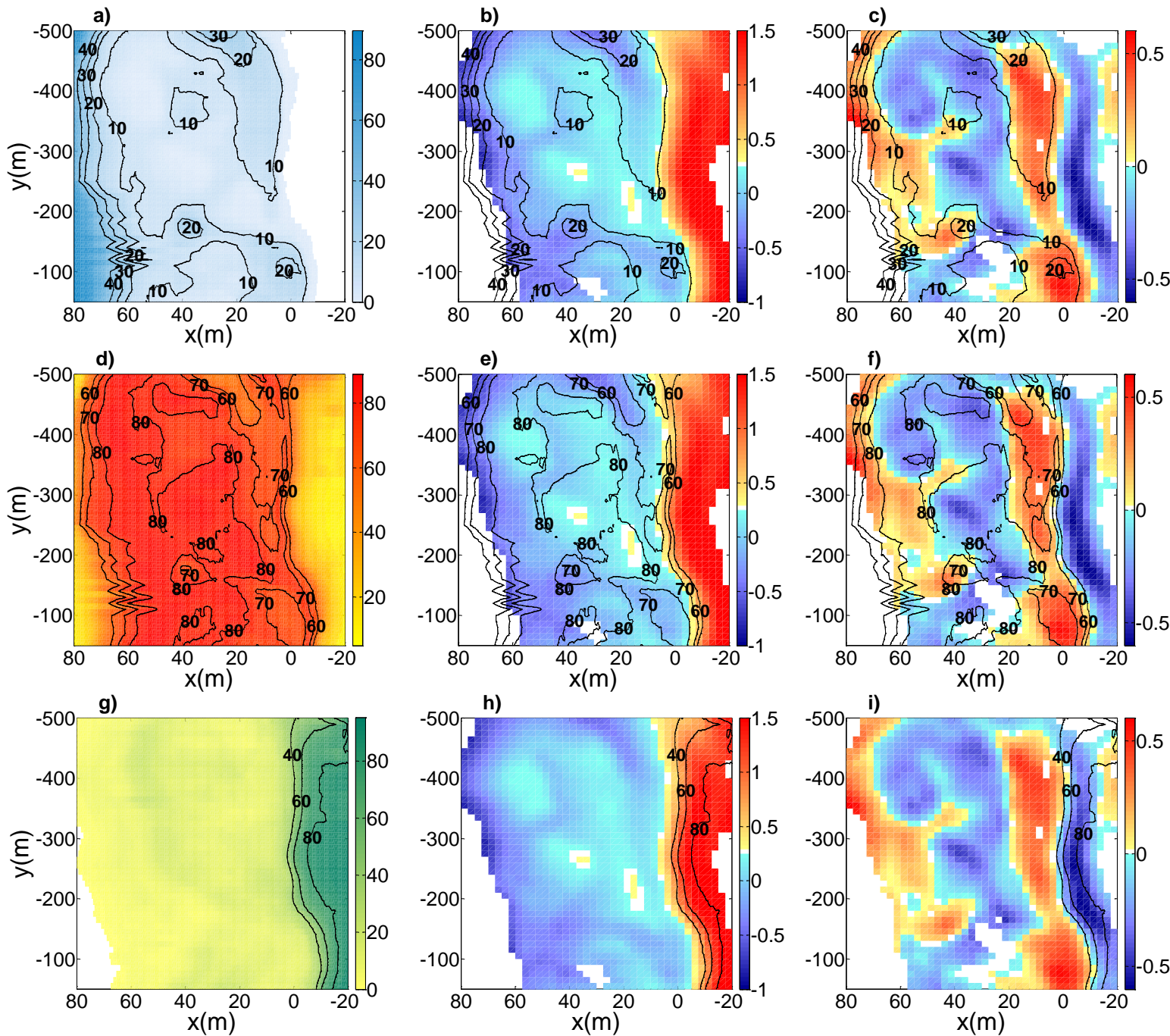


Figure 22. The (a) shoaling zone (blue), (d) surf zone (yellow) and (g) swash zone (green) distribution of Period 2. The contour lines of the (b) shoaling zone, (e) surf zone and (h) swash zone are plotted on the DEM of the beginning of Period 1. In addition, the (c) shoaling, (f) surf and (i) swash contour lines are also plotted on the corresponding Difference Model.

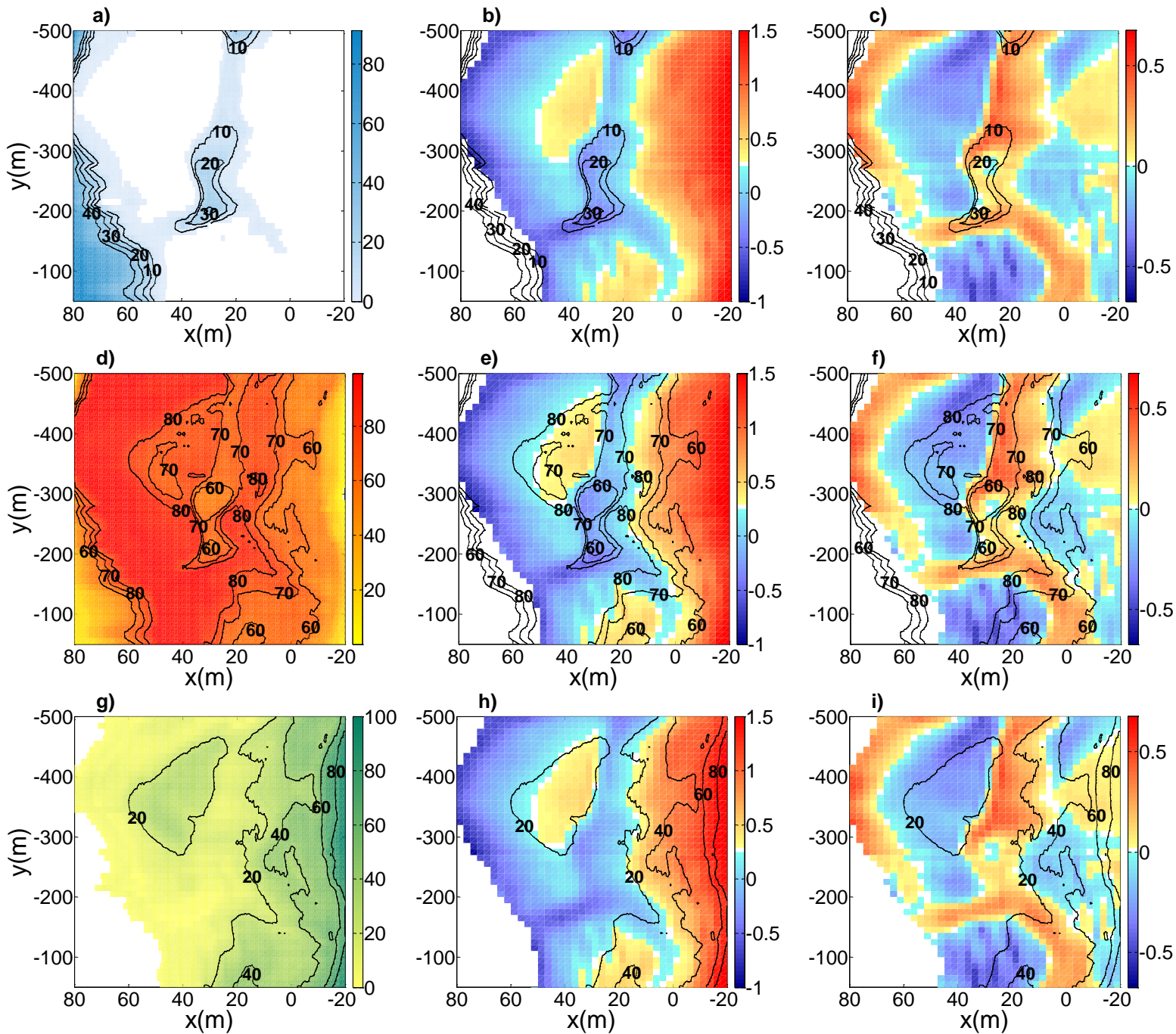


Figure 23. The (a) shoaling zone (blue), (d) surf zone (yellow) and (g) swash zone (green) distribution of Period 3. The contour lines of the (b) shoaling zone, (e) surf zone and (h) swash zone are plotted on the DEM of the beginning of Period 1. In addition, the (c) shoaling, (f) surf and (i) swash contour lines are also plotted on the corresponding Difference Model.

4.2.2 ALONGSHORE UNIFORMITY

The spatial variability of the morphodynamic zones is determined using the methodology of Plant et al. (1999) (section 3.1 and Table 6). The two periods with high energetic wave conditions, Period 2 and 3, show a relatively alongshore uniform distribution of morphodynamic zone processes. During Period 2, the fraction of the total variance that is alongshore uniform is $s^2/S^2 = 0.69$ for the shoaling zone, $s^2/S^2 = 0.82$ for the surf zone and $s^2/S^2 = 0.90$ for the swash zone. The alongshore uniformities of the morphodynamic zones are lower during Period 3 compared to Period 2 with $s^2/S^2 = 0.59$ for the surf zone, $s^2/S^2 = 0.85$ for the swash zone and $s^2/S^2 = 0.34$ for the shoaling zone. The initial three-dimensional morphology of Period 3 (Table 5) probably causes the fraction of the total variance that was alongshore uniform to be smaller compared to Period 2, that starts with a more alongshore uniform morphology (Table 5). The fraction of the total variance that was alongshore uniform for the morphodynamic zones of Period 1 are relatively low compared to Period 2 and 3 with $s^2/S^2 = 0.25$ for the surf zone, $s^2/S^2 = 0.37$ for the swash zone and $s^2/S^2 = 0.42$ for the shoaling zone. The low energetic wave conditions during Period 1 caused the waves to be more affected by relatively small changes in water depth, resulting in a more alongshore variable distribution.

Table 6. The total variation S^2_{tot} , two-dimensional variation s^2_{2D} and the ratio between s^2_{2D} and S^2_{tot} of the shoaling zone, surf zone and swash zone distribution for the three periods.

	Period 1			Period 2			Period 3		
	shoaling	surf	swash	shoaling	surf	swash	shoaling	surf	swash
$S^2_{tot} (m^2)$	358.38	264.71	288.12	275.71	527.97	698.91	563.58	447.46	440.41
$s^2_{2D} (m^2)$	151.52	67.34	105.85	191.48	431.86	627.54	189.91	265.71	373.15
s^2_{2D} / S^2_{tot}	0.42	0.25	0.37	0.69	0.82	0.90	0.34	0.59	0.85

4.2.3 THE CROSS-SHORE RELATION BETWEEN THE MORPHODYNAMIC ZONE DISTRIBUTION AND DIFFERENCE MODEL

This section discusses the morphodynamic zone distributions and the observed changes in morphology. Price and Ruessink (2008) explained intertidal beach changes by the relative occurrence of the morphodynamic zone processes in one cross-shore profile, as is shown in Figure 2 and Figure 3. A more or less similar comparison can be made by alongshore averaging the morphodynamic zone distributions and the corresponding Difference Models. However, this approach differs from Price and Ruessink (2008) as averaged area measurements are used instead of data from a single cross-shore profile.

The Difference Models, the alongshore averaged Difference Models and the alongshore averaged morphodynamic zone distributions are displayed in Figure 24. The alongshore averaged DM profiles do not always completely cover the original DM because the alongshore averaged profiles were only calculated for cross-shore locations where more than 50% of the alongshore observations were available. The alongshore averaged DMs do not all show a closed system, as the most seaward and shoreward average does not end at zero. This indicates that either alongshore processes were involved or that the measurements did not extend sufficiently far enough.

The steepening of the beach face during Period 1 is clearly visible in the alongshore averaged DM between $x = 10m$ and $x = -10m$. The erosion of the lower beach face, between $x = 10m$ and $x = -5m$, was primarily caused by breaking waves while the sedimentation at the upper beach face, between $x = -5m$ and $x = -15m$, was induced by swash zone processes. At the seaward side of the alongshore averaged DM the sedimentation on top of the intertidal bar is visible, between $x = 60m$ and $x = 50m$, but the measurements did not extend seaward enough to capture the erosion on the seaward side of the intertidal bar. There are no further changes visible in the alongshore averaged

DM. The sedimentation at the landward side of the intertidal bar, that induced onshore bar migration, is canceled out in the alongshore averaged DM due to its alongshore variability.

The offshore bar migration during Period 2 is visualized in the alongshore averaged DM by erosion between $x = 20\text{m}$ and $x = 60\text{m}$ and sedimentation seaward of $x = 60\text{m}$. Again, the measurements did not extend seaward sufficiently to capture the entire sedimentation seaward of the intertidal bar. The bar erosion is induced by surf zone processes and sediment is deposited at the location where the residence time of the surf zone diminishes in favor of that of the shoaling zone. The flattening of the beach face is also clearly visible in the alongshore averaged DM by erosion between $x = 5\text{m}$ and $x = -20\text{m}$ and deposition of the eroded sediment at the lower beach face, between $x = 20\text{m}$ and $x = 5\text{m}$. The transition between erosion and sedimentation at the lower beach face corresponds to the intersection between the relative occurrence of the surf zone and the swash zone at $x = 5\text{m}$. This indicates that the beach face eroded under swash conditions and the sediment was deposited seaward of the location where the residence time of the surf zone diminished in favor of the swash zone.

The alongshore averaged morphodynamic zone distribution of Period 3 shows a similar distribution as during Period 2. Surf zone processes dominate the intertidal beach, relatively high occurrences of swash are visible at the beach face and the shoaling zone is active seaward of the intertidal bar. The offshore migration of the intertidal bar is visualized in the alongshore averaged DM between $x = 25\text{m}$ and $x = 65\text{m}$ and is induced by surf zone processes. The relative occurrence of the surf zone and the swash zone cross each other at $x = 15\text{m}$, but there is no transition visible between sedimentation at the lower beach face and erosion at the upper beach face, as was observed during Period 2. The alongshore averaged DM does not display the erosion of the upper beach face because there was also sedimentation at the beach face ($y = -300\text{m}$ and $y = -450\text{m}$), which counteracts the erosion in the alongshore averaged DM. The sedimentation of the rip channel, which led to the disappearance of the rip channel, is also not displayed in the alongshore averaged DM. Compared to the other periods, the fraction of the total variance that was alongshore uniform is the lowest for the DM of period 3 (Table 5). This indicates that the observed changes in intertidal beach morphology are relatively alongshore non-uniform and that the alongshore averaged DM does not represent all observed changes nor does the alongshore averaged morphodynamic zone distribution explain the shape of the alongshore averaged DM.

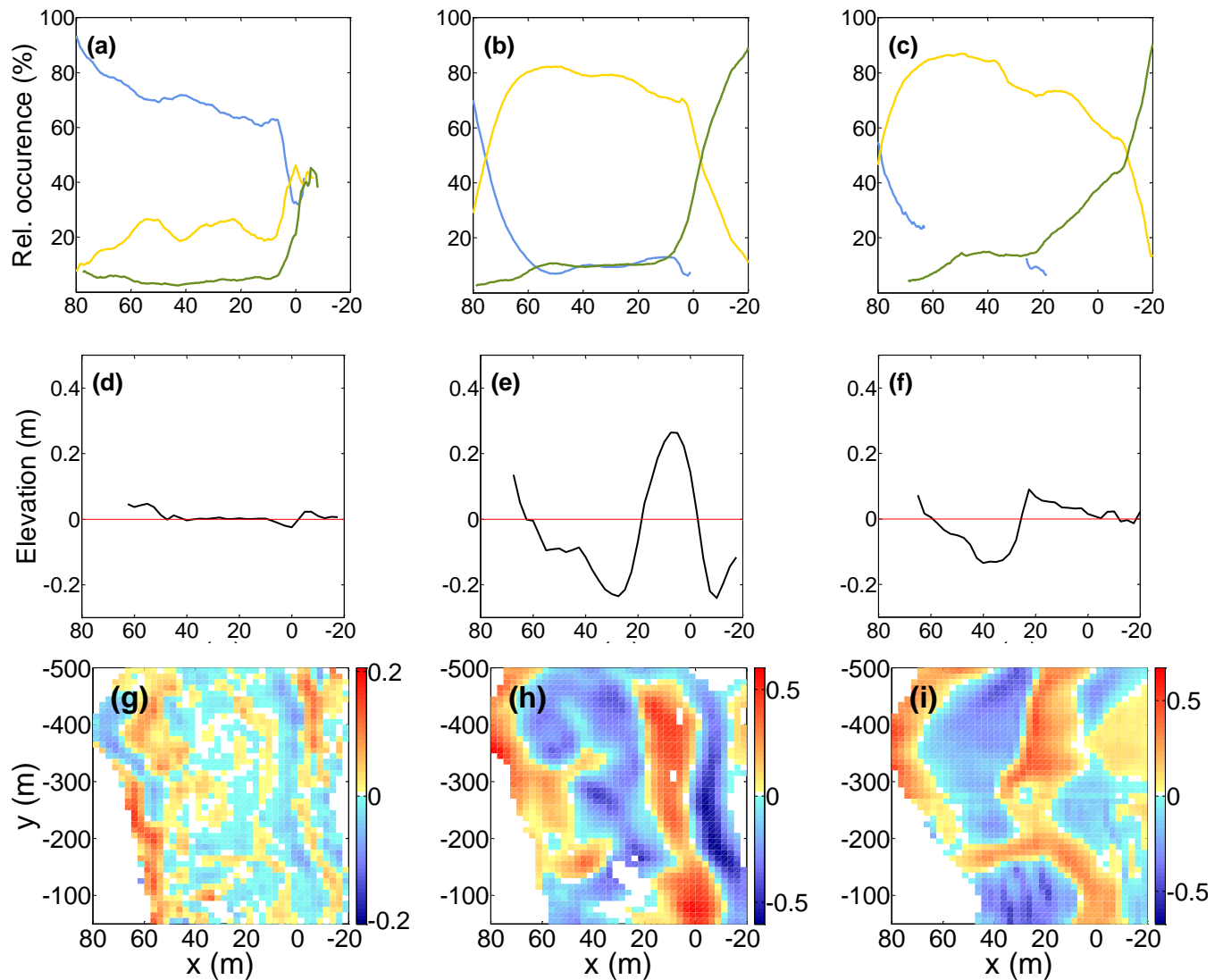


Figure 24. The Difference Model, alongshore averaged Difference Model and the alongshore averaged morphodynamic zone distribution for Period 1 (a, d, g), Period 2 (b, e, h) and Period 3 (e, f, i).

The decay of the rip channel during Period 3 is the only three-dimensional change observed during the field campaign that is induced by the decay of a three-dimensional feature (section 1). In section 4.2.1 there was no clear relation found between the sedimentation in the rip channel and the contour lines of the morphodynamic zones. The disappearance of the rip channel and the morphodynamic zone distribution is examined in more detail in order to determine whether the decay of the rip channel was indeed not induced by morphodynamic zone processes. The alongshore averaged Difference Model and the alongshore averaged morphodynamic zone distribution are displayed in Figure 25 for three selected areas: one area north of the rip channel, the area of the rip channel, and one area south of the rip channel (Figure 25). The distribution of the relative occurrence of the morphodynamic zones are more or less similar for the three selected areas. Swash zone processes were active on the intertidal bar and on the upper beach face. The surf zone was active on the lower beach face, and on the intertidal bar. Furthermore, Shoaling processes were active seaward of the intertidal bar and in the intertidal trough. The area north and south of the rip channel showed similar erosion and sedimentation patterns. The beach face was eroded under swash conditions and the sediment was deposited at the lower beach face. The intertidal

bar migrated offshore under the prevailing surf zone conditions. The measurements of the southern area did not extend seaward enough to capture the deposition of the eroded intertidal bar at the seaward side. Even though the alongshore averaged morphodynamic zone distribution of the rip channel area was almost similar to the distribution in the northern and southern area, the observed changes are different. The alongshore averaged DM of the rip channel shows erosion of the beach face, induced by swash zone processes, followed by a relatively large region of sedimentation. This sedimentation event cannot be explained by a difference in the relative occurrence of the morphodynamic zones as the relative occurrence is equal to the occurrences of areas in the north and south. So the cross-shore processes of the morphodynamic zones are unable to explain the decay of the rip channel, which is in line with the drawn hypothesis (section 1). In addition, the alongshore averaged DM of the rip channel is far from a closed system which also suggest that alongshore processes were involved.

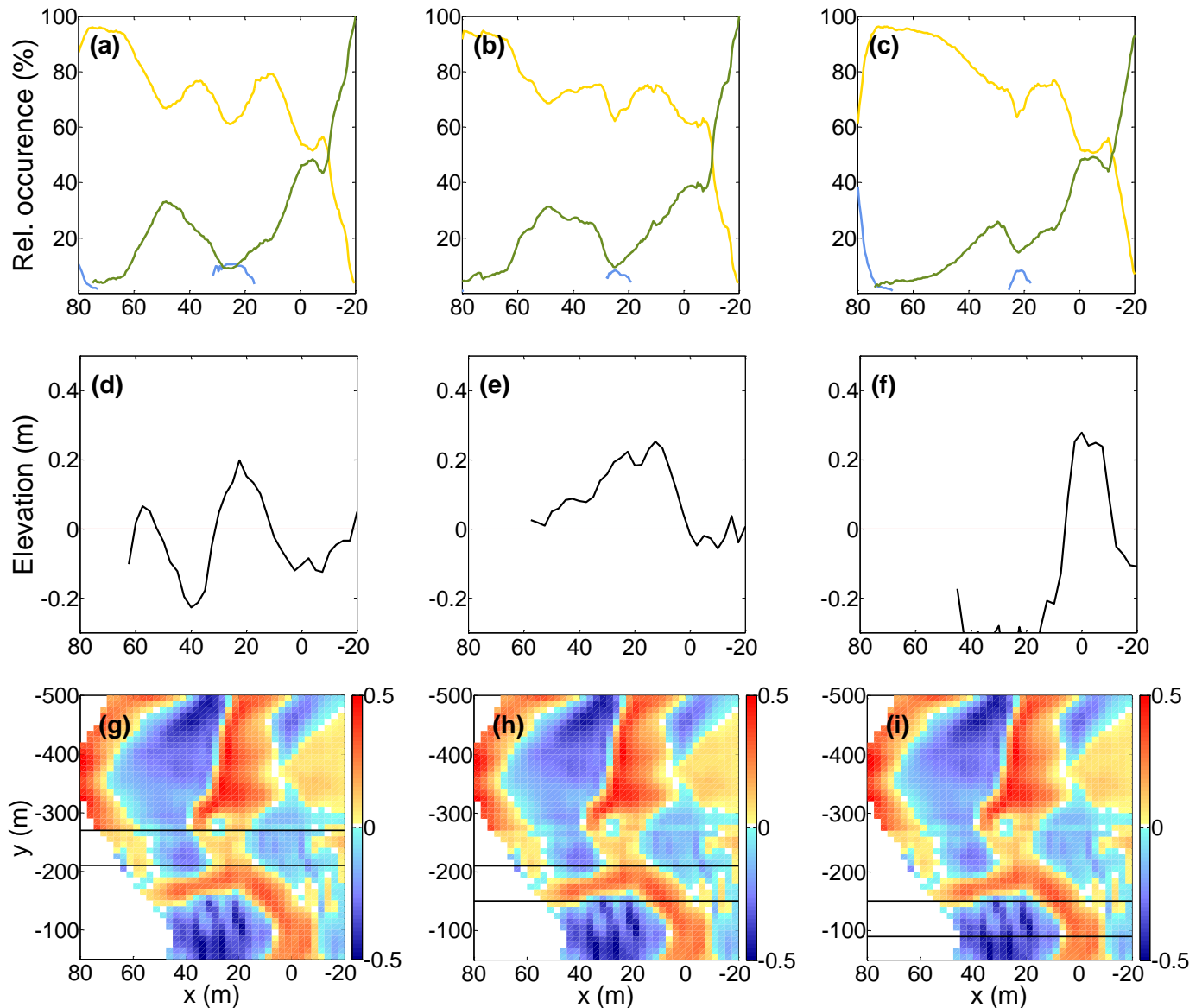


Figure 25. The DEM selected area of the rip channel (h), north of the rip channel (g) and south of the rip channel (i) and the corresponding alongshore averaged DEM selection and alongshore averaged morphodynamic zone distribution for the specific area.

4.2.4 ALONGSHORE VARIABILITY OF THE MORPHODYNAMIC ZONE DISTRIBUTIONS

The cross-shore variation in the intensity of the relative occurrence of morphodynamic zones is caused by the morphology and the wave energy conditions (Price and Ruessink, 2008). However, the intensity of the morphodynamic zone processes also varies alongshore (Figure 21, Figure 22 and Figure 23). In this section two possible causes of the alongshore variability in intensity of morphodynamic zone processes will be discussed: the alongshore variability in offshore bathymetry and the alongshore variation of the intertidal beach morphology.

Waves arriving at the intertidal zone may vary alongshore in height and intensity as a result of possible alongshore variation in water depth due to the offshore bathymetry. The offshore bathymetry that is used as input for the model (section 3.2.1) is displayed in Figure 26a. The outer bar does not show significant alongshore variation in height, in contrary to inner bar. Figure 26b shows three cross-shore profiles, one intersecting the top ($y = -250\text{m}$), one north and one south of the inner bar ($y = -400\text{m}$ and $y = -100\text{m}$). The maximum alongshore difference in height of the inner bar is 0.50m , which could induce alongshore variations in wave height. The wave height landward of the inner bar is investigated (at $x = 115\text{m}$) to determine the effect of the alongshore variation in inner bar height. Figure 26c shows the wave height at $x = 115\text{m}$ for both a high water ($h = 1.13\text{m N.A.P.}$) and a low ($h = -0.25\text{m N.A.P.}$) condition during the high energetic wave conditions of Period 2. The relatively high part of the inner bar, at $y = -275$, causes a decrease in landward wave height. During high water, the wave height landward of the inner bar decreased with a maximum of 10%. The wave height decreased even more during low water, with a maximum decrease of 33%. During these low water level conditions, a second inner bar in the northern part of the area causes a similar but smaller effect, with a maximum decrease of 8.5%.

It can therefore be said that the offshore bathymetry does influence the alongshore variation in intensity of the incoming waves. This influence is relatively high during low water levels, with a maximum wave height decrease of 33% compared to 10% during high water levels. However, the pattern of the obtained morphodynamic zone distributions (Figure 21, Figure 22 and Figure 23) does not correspond to this effect. It could therefore be assumed that the influence of the alongshore variation in bathymetry on the morphodynamic zone distribution is small and that the offshore bathymetry does not have significant influence on the results of this study.

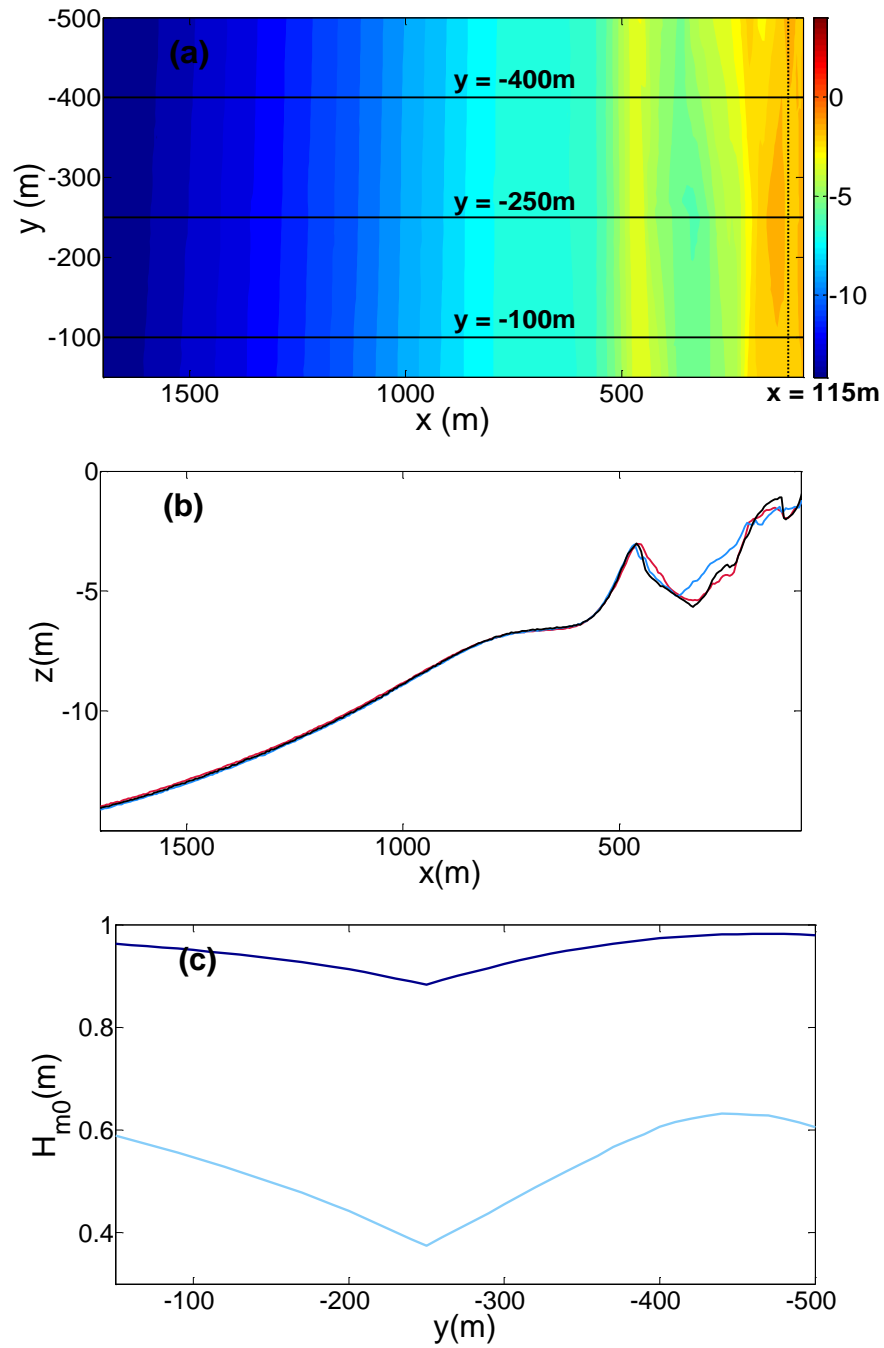


Figure 26. The (a) bathymetry that is used as input of the model and the three locations of the (b) cross-shore profiles. The (b) wave height at $x = 115\text{m}$ for both high (dark blue) and low (light blue) water during the high energetic wave conditions of Period 2.

The morphodynamic zone distributions (Figure 21, Figure 22 and Figure 23) already indicated that the spatial variability in relative occurrence of morphodynamic zones is related to the spatial variability of the intertidal beach morphology. Two clear situations whereby the intensity of the morphodynamic zones varies alongshore are highlighted for illustration. First, the surf zone distribution of Period 1 (Figure 27a) and second, the swash distribution of Period 2 (Figure 27b).

Comparing the surf zone distribution of Period 1 with the initial morphology indicates that the relatively high occurrences of surf processes are located on the relatively high parts of the intertidal bar. In order to see if these alongshore variations in surf zone processes also cause alongshore variation in intertidal beach changes, two cross-shore locations are investigated. For the two locations, the relative occurrence of surf processes (Figure 28a), the changes in morphology (Figure 28b) and the initial morphology across the intertidal beach (Figure 28c) are shown. The intertidal bar at location 1 lies further onshore compared to the bar at location 2 which causes the surf zone processes at location 1 to occur further offshore compared to location 2. This results in relatively further offshore located sedimentation at the intertidal bar on location 1 and relatively more onshore sedimentation at location 2. A similar process is visible at the beach face as the beach face on location 2 is located further onshore compared to location 1 which means that the beach face erosion is also located further onshore on location 2 compared to location 1.

For Period 2, the swash zone distribution is investigated for two locations (Figure 27b and Figure 29). The relatively high occurrence of swash is located further offshore at location 3 compared to location 4 which is caused by the fact that the upper beach face of location 3 is also located further offshore compared to location 4. This causes alongshore variation in beach face erosion.

To conclude, the offshore bathymetry does not significantly influence the height and intensity of the incoming waves, but the alongshore variation in intertidal beach morphology is the main cause of the alongshore variation in morphodynamic zone distribution. Therefore, given the intertidal beach morphology, spatial variability in observed changes in intertidal beach morphology can - in this study - be explained by the spatial variability of the morphodynamic zone distribution.

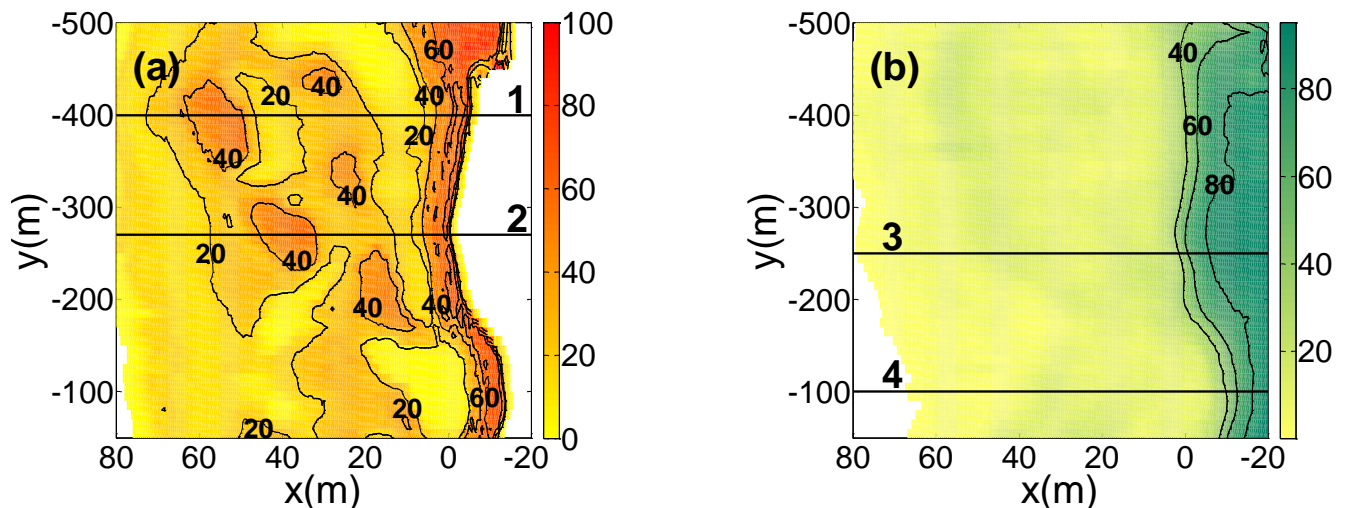


Figure 27. The surf zone distribution of Period 2 with the two locations (1 and 2) of the cross-shore profiles and (b) the swash zone distribution of Period 2 with the two locations (3 and 4) of the cross-shore profiles that were investigated.

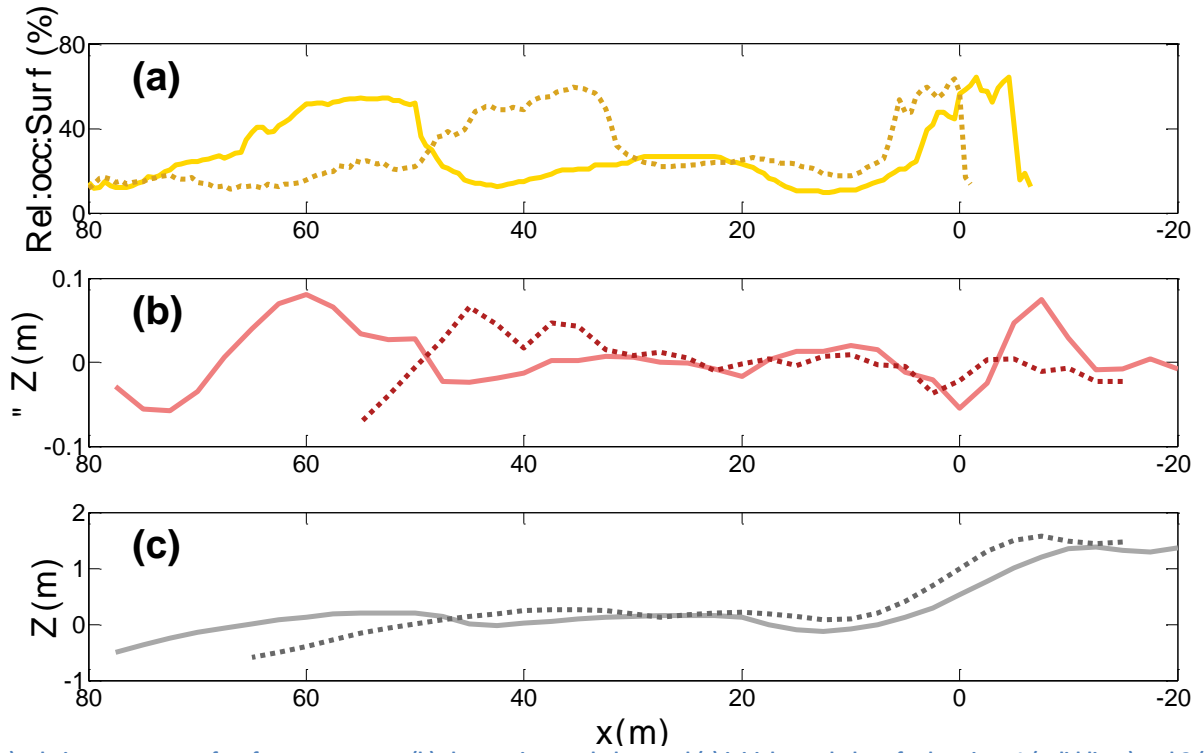


Figure 28. The (a) relative occurrence of surf zone processes, (b) changes in morphology and (c) initial morphology for locations 1 (solid lines) and 2 (dashed lines) during Period 1.

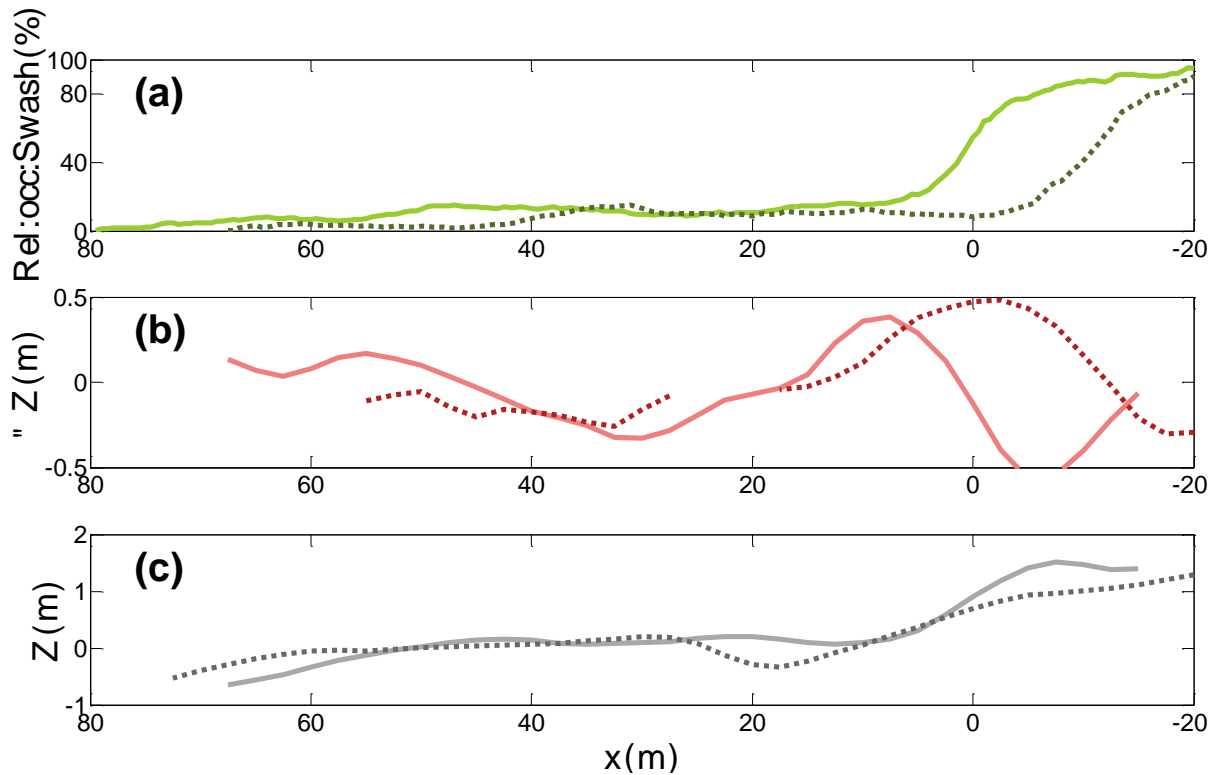


Figure 29. The (a) relative occurrence of swash zone processes, (b) changes in morphology and (c) initial morphology for locations 1 (solid lines) and 2 (dashed lines) during Period 2.

5 CONCLUSION

This study extended existing work on the use of the morphodynamic zone approach of Price and Ruessink (2008) by determining if three-dimensional changes in intertidal beach morphology can be explained by the relative distribution of morphodynamic zone processes. A fieldwork was conducted from 28 September to 31 October 2011 at Egmond aan Zee, the Netherlands, to map the intertidal beach morphology and determine the changes in intertidal beach morphology. The measured morphology was used as input for the cross-shore wave transformation model coupled to an inner surf zone model. This model provided estimation on wave properties that were used to derive the morphodynamic zone boundaries. The modeled wave height satisfactory corresponded to the measurements. However, the wave height became slightly over predicted towards the end of the selected period. This offset was probably caused by changes in offshore morphology that were induced by high energetic wave conditions and were not incorporated as input for the model. In addition, the assumption that the morphology changes linearly over time has shown to be incorrect and the thereby induced errors influenced the results and accuracy of the model.

Consistent with Price and Ruessink (2008), it was found that low energetic wave conditions enhance the intertidal morphology and cause onshore bar migration, whereas high energetic wave conditions cause flattening of the intertidal morphology and offshore bar migration. Moreover, high energetic wave conditions with oblique incident waves were, in combination with an initial alongshore varying morphology, able to destruct the morphological pattern by the decay of a three-dimensional feature present in the initial beach morphology.

The alongshore uniformity, which is the fraction of the total variation that is alongshore uniform, was tested for the morphology and changes in morphology, using the approach of Plant et al. (1999). It was found that low energetic wave conditions induce the alongshore uniformity of the morphology and enhance morphological features, like the berm, bar and trough. These morphological features also cause an increase in alongshore variation of the intertidal morphology, but their main pattern is shore parallel thus induce an increase in alongshore uniformity. During low energetic wave conditions, the alongshore uniformity decreases because the morphological features are flattened. Overall, the alongshore varying beach width and the rip channels causes the alongshore uniformity of the intertidal beach morphology to be unexpectedly low because the main pattern of the morphology is shore parallel.

The morphodynamic zone distributions show an alongshore variable distribution. This alongshore variation in morphodynamic zone distributions is caused by the alongshore variation of the initial morphology and therefore induces alongshore variation in the observed intertidal beach changes. All the observed changes in intertidal beach morphology were three-dimensional, as their alongshore uniformity was below 0.5. This indicates that the alongshore variation of the observed intertidal beach changes induced more than 50% of the total variation.

Given the morphology, the alongshore variation in intensity of morphodynamic zones can explain three-dimensional changes induced by the on/offshore bar migration and enhancing/flattening of the morphology. Destruction of morphological patterns, induced by the decay of three-dimensional features, cannot be explained by the morphodynamic zone distribution as alongshore processes are involved.

6 RECOMMENDATIONS

During the field campaign, the intertidal beach morphology was measured with an RTK-GPS system mounted on a quad. Due to the differences in weight between the two quad operators the RTK-GPS base height differed, which resulted in an offset in the elevation data. It is therefore strongly recommended that future bathymetric measurements with a similar system are conducted whereby the added weight of the quad and operator is identical each measurement to avoid these kind of offset errors.

The assumption that the morphology changes linearly over time has proven to be incorrect. More frequent bathymetric measurements during the period of interest would improve the model performance as it reduces the interpolation errors between the observations.

During the field campaign, the seaward measurements were sometimes limited due to the high water levels. This caused not all the changes in the morphology to be mapped. It would therefore be beneficial to obtain bathymetry measurements further offshore to map all the changes in the intertidal beach morphology. In an ideal situation these measurements would extend so far that they replace the static offshore bathymetry that was retrieved from Rijkswaterstaat. This would improve the modeled wave propagation and would therefore induce the model's accuracy.

To extend the current work on the morphodynamic zone approach, it would be of interest to determine the alongshore as well as cross-shore sediment transport and to measure alongshore current velocities to better quantify alongshore processes involved.

7 BIBLIOGRAPHY

- Aagaard, T., Hughes, M., Moller-Sorensen, R., & Andersen, S. (2006). Hydraulics and sediment fluxes across an onshore migrating intertidal bar. *Journal of Coastal Research*, 22, 247-259.
- Aagaard, T., Kroon, A., Andersen, S., Moller Sorensen, R., Quartel, S., & Vinther, N. (2005). Intertidal beach change during storm conditions: Egmond, The Netherlands. *Marine Geology*, 218, 65-80.
- Aarninkhof, S., & Roelvink, J. (1999). Argus-based monitoring of intertidal beach morphodynamics. *Proc. coastal Sediments* (pp. 2429-2444). New York: ASCE.
- Battjes, J., & Janssen, J. (1978). Energy loss and set-up due to breaking of random waves. *Proc. 16th Int. Conf. on Coastal Engineering* (pp. 2429-2444). New York: ASCE.
- Butt, T., Russell, P., Puleo, J., Miles, J., & Masselink, G. (2004). The influence of bore turbulence in sediment transport in the swash and inner surf zones. *continental Shelf Research*, 24, 757-771.
- Cleveland, W., & Devlin, S. (1988). Locally weighted regression: An approach to regression analysis by local fitting. *Journal of the American Statistical Association*, 83, 596-610.
- Deigaard, R. (1993). A note on three-dimensional shear stress distribution in a surf zone. *Journal of Coastal Research*, 20, 157-171.
- Duncan, J. (1981). An empirical investigation of breaking wave produced by towed hydrofoil. *Proc. R. Soc. Lond. A*, 377, 331-348.
- Gallagher, E., Elgar, S., & Guza, R. (1998). Observations of sand bar evolution on a natural beach. *Journal of Geophysical Research*, 103, 3203-3215.
- Gallagher, E., Elgar, S., & Thornton, E. (1998). Megaripple migration in a natural surf zone. *Nature*, 251, 165-169.
- Lafon, V., De Melo Apoluceno, D., Dupuis, H., Michel, D., & Froidefond, J. (2004). Morphodynamics of nearshore rhythmic sandbars in a mixed energy environment (SW France): I. Mapping beach changes using visible satellite imagery. *Estuarine, Coastal and Shelf Science*, 61(2), 289-299.
- Masselink, G. (1993). Simulating the effects of tides on beach morphodynamics. *Journal of Coastal Research*, 15, 180-197.
- Masselink, G., Kroon, A., & Davidson-Arnott, R. (2006). Morphodynamics of intertidal bars in wave-dominated coastal settings - A review. *Geomorphology*, 73, 33-49.
- Plant, N. G., Holland, T. K., & Puleao, J. A. (2002). Analysis of the scale of errors in nearshore bathymetric data. *Marine Geology*, 191, 71-86.
- Plant, N., Holman, R., & Freilich, M. (1999). A simple model for interannual sandbar behavior. *Journal of geophysical research*, 107(C7), 15755-15776.
- Price, T. D., & Ruessink, B. G. (2008). Morphodynamic zone variability on a microtidal barred beach. *Marine Geology*, 251, 98-109.

- Quartel, S., Ruessink, B., & Kroon, A. (2007). Cross-shore behaviour of an intertidal bar-trough system. *Earth Surface Processes and Landforms*, 32(9), 1293-1307.
- Rijkswaterstaat. (2012, December 12). Uw vraag aan Rijkswaterstaat [Incident: 121210-000231].
- Ruessink, B., & Van Enckevort, I. (2003). Video observations of nearshore bar behaviour. Part 2: alongshore non-uniform variability. *Continental Shelf Research*, 23, 513-532.
- Ruessink, B., Van Enckevort, I., & Davidson, M. (2000). Analysis of observed two- and three-dimensional nearshore bar behaviour. *Marine Geology*, 169, 161-183.
- Short, A. (1985). Rip-current type, spacing and persistence, Narrabeen Beach, Australia. *Marine Geology*, 65, 47-71.
- Sonu, C., & Russell, R. (1967). Topographic changes in the surf zone profile. *Proceedings of the 10th International Conference on Coastal Engineering* (pp. 502-524). New York: ASCE.
- Stive, M., & De Vriend, H. (1994). Shear stress and mean flow in shoaling and breaking waves. *Proceedings of the 24th International Conference on Coastal Engineering* (pp. 594-608). New York: ASCE.